Initial growth of the Northern Lhasaplano, Tibetan Plateau in the early Late Cretaceous (ca. 92 Ma)

Wen Lai[1], Xiumian Hu[1,†], Eduardo Garzanti[2], Gaoyuan Sun[1,3], Carmala N. Garzione[4], Marcelle BouDagher Fadel[5], and Anlin Ma[1]

[1]*State Key Laboratory of Mineral Deposits Research, School of Earth Sciences and Engineering, Nanjing University, Nanjing 210023, China*

[2]*Department of Earth and Environmental Sciences, Università di Milano-Bicocca, Milano 20126, Italy*

[3]*College of Oceanography, Hohai University, Nanjing 210098, China*

[4]*Department of Earth and Environmental Sciences, University of Rochester, Rochester, New York 14627, USA*

[5]*Department of Geological Sciences, University College London, London WC1E6BT, UK*

ABSTRACT

Constraining the growth of the Tibetan Plateau in time and space is critical for testing geodynamic models and climatic changes at the regional and global scale. The Lhasa block is a key region for unraveling the early history of the Tibetan Plateau. Distinct from the underlying shallow-marine limestones, the Jingzhushan and Daxiong formations consist of conglomerate and sandstone deposited in alluvial-fan and braided-river systems. Both units were deposited at ca. 92 Ma, as constrained by interbedded tuff layers, detrital zircons, and micropaleontological data. Provenance and paleocurrent analyses indicate that both units were derived from the same elevated source area located in the central-northern Lhasa block. These two parallel belts of coeval conglomerates record a major change in paleogeography of the source region from a shallow seaway to a continental highland, implying initial topographic growth of an area over 160,000 km², named here the Northern Lhasaplano. The early Late Cretaceous topographic growth of the Northern Lhasaplano was associated with the demise of Tethyan seaways, thrust-belt development, and crustal thickening. The same paleogeographic and paleotectonic changes were recorded earlier in the Northern Lhasaplano than in the Southern Lhasaplano, indicating progressive topographic growth from north to south across the Bangong-Nujiang suture and Lhasa block during the Cretaceous. Similar to the Central Andean Plateau, the Northern Lhasaplano developed by plate convergence above the oceanic Neo-Tethyan subduction zone before the onset of the India-Asia collision.

†Corresponding author: huxm@nju.edu.cn.

INTRODUCTION

The Tibetan Plateau, with an average elevation of ~5000 m, is the world's highest and widest orogenic plateau, and exerts a major influence on the Asian monsoon, global climate change, and regional distribution of living species (Raymo and Ruddiman, 1992; Molnar et al., 1993; An et al., 2001; Dupont-Nivet et al., 2007; Deng et al., 2011). Constraining the surface-uplift history of the Tibetan Plateau is critical for understanding the geodynamic mechanisms that build orogenic plateaus, as well as the plateau's influence on regional and global climate (Chung et al., 1998; Rowley and Currie, 2006; Wang et al., 2008; 2014; Xu et al., 2015). The spectacular angular unconformity separating folded Mesozoic strata of the Lhasa block (Fig. 1A) from the overlying, weakly deformed 60–52 Ma Linzizong volcanic succession (Pan et al., 2004; Zhu et al., 2015), led to the inference of an Andean-style orogenic episode associated with the Gangdese arc (England and Searle, 1986). Structural restorations suggest that >50% crustal shortening of the Lhasa block took place during the Cretaceous (Murphy et al., 1997; Kapp et al., 2007a; Volkmer et al., 2007), leading to the hypothesis that a "Lhasaplano," a narrow high-elevation plateau similar in size to the modern Andean Plateau (Altiplano), developed before the India-Asia collision (Kapp et al., 2005). Wang et al. (2008) argued in favor of a proto-Tibetan plateau and provided stratigraphic and thermochronological evidence of surface uplift of the Lhasa and southern Qiangtang terranes before 40 Ma. Such a scenario has led to new important questions: if an ancient plateau existed before the India-Asia collision, then how did it form, and when and where did it start to grow?

Most previous reconstructions of Tibetan Plateau growth have focused on paleoelevation estimates and low-temperature thermochronology. Stable isotopes in lacustrine carbonates suggest that the basins surrounding the Gangdese Mountains in the southern Lhasa terrane had reached an elevation >4500 m since India-Asia collision (Ding et al., 2014). Low-temperature thermochronology reveal that the central and northern Lhasa terranes experienced rapid to moderate cooling and exhumation between 85 and 45 Ma (Hetzel et al., 2011; Rohrmann et al., 2012). These studies shed light on the evolution of the Tibetan Plateau, but do not establish when and where the ancient plateau was initially uplifted.

The aim of the present study is to corroborate or falsify the early growth of a "Lhasaplano," following the Qiangtang-Lhasa collision but predating the India-Asia collision. To this goal we investigated the spatial distribution, depositional age, and paleogeographic setting of non-marine Late Cretaceous strata in the Lhasa block. We carried out detailed multi-technique sedimentological and provenance analysis based on gravel composition, sandstone petrology, paleocurrent directions, detrital zircon U-Pb ages and Hf isotopes to provide evidence for erosion of the central and northern Lhasa terranes, and resolve the timing and spatial distribution of surface uplift.

GEOLOGICAL BACKGROUND

The Tibetan Plateau formed by the progressive accretion of a series of microcontinents (Fig. 1A), including the Lhasa block in the south and the Qiangtang block to the north, welded along the Bangong-Nujiang suture zone (BNSZ). The Lhasa block (Fig. 1A) can be subdivided into southern, central, and northern terranes, separated by the Shiquanhe-Nam Co Mélange zone (SNMZ) and by the Luobadui-Milashan Fault (LMF), respectively (Zhu et al., 2011b). The southern Lhasa terrane (Fig. 1B) is characterized by Late Triassic to Paleogene Gangdese plutonic and Paleogene Linzizong

https://doi.org/10.1130/B35124.1; 10 figures; Data Repository item 2019138.

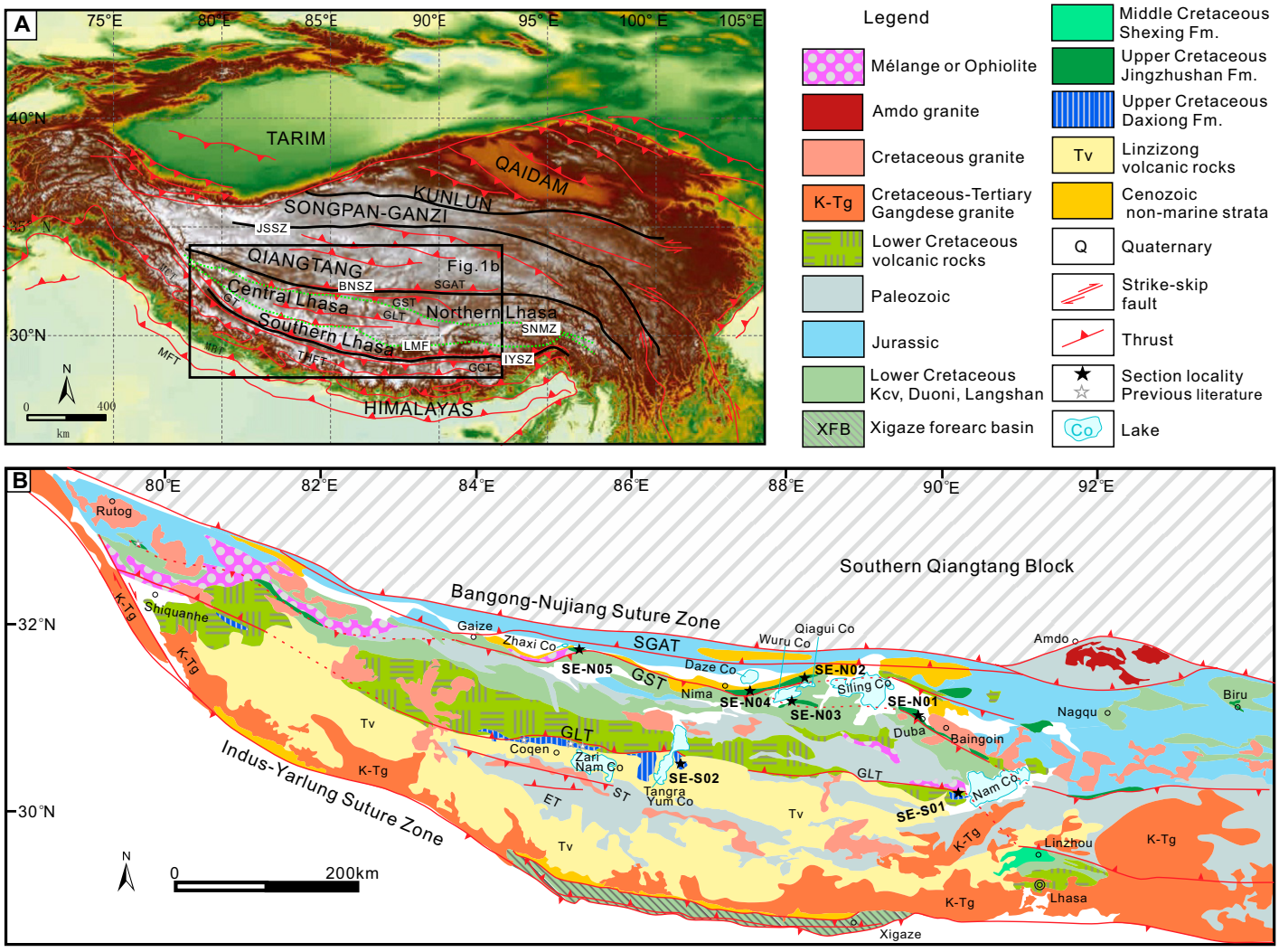

Figure 1. (A) Tectonic map of the Tibetan Plateau (modified after Zhu et al., 2011b and Wang et al., 2014). (B) Sketch geological map of the Lhasa block (modified after Pan et al., 2004 and Kapp et al., 2003). Previously studied sites of the Daxiong Formation in the Coqen basin (Sun et al., 2015a) and of the Jingzhushan Formation near Rutog (Li et al., 2014a) are shown. JSSZ—Jinsha suture zone; SNMZ—Shiquan River-Nam Co Mélange zone; LMF—Luobadui-Milashan Fault; SGAT—Shiquanhe-Gaize-Amdo thrust; GST—Gaize-Siling Co thrust; GLT—Gugu La thrust; ST—Shibaluo thrust; ET—Emei La thrust; MCT—Main Central thrust; MBT—Main Boundary thrust; THFT—Tethyan Himalaya fold-thrust belt; GCT—Great counter thrust; IYSZ—Indus-Yarlung Zangbo Suture zone; BNSZ—Bangong-Nujiang suture zone; GT—Gangdese thrust.

volcanic rocks yielding zircons with εHf(t) >10 (Chu et al., 2006; Ji et al., 2009; Zhu et al., 2011b, 2015). Along the southern margin of the Gangdese magmatic arc, thick deep-water turbidites were deposited in the Xigaze forearc basin during Albian to Santonian (An et al., 2014; Orme and Laskowski, 2016). The central Lhasa terrane (Fig. 1B) includes Precambrian crystalline basement (Pan et al., 2004), very low-grade Carboniferous metasediments, Permian limestones, and Jurassic siliciclastic successions. A suit of volcano-sedimentary successions, yielding zircons with negative $\varepsilon_{Hf}(t)$, accumulated during the Early Cretaceous (Zhu et al., 2011B), whereas the non-marine Daxiong Formation was deposited in the Coqen basin during the Late Cretaceous (Sun et al., 2015a).

The northern Lhasa terrane (Fig. 1B) comprises >4 km of Late Jurassic to Early Cretaceous marginal-marine and deltaic strata (XZBGM, 1993), overlain by continental deposits of the Late Cretaceous Jingzhushan Formation (Kapp et al., 2007b; Zhang et al., 2011). Cretaceous plutonic and volcanic rocks also occur (Zhu et al., 2011b).

The BNSZ, traced for ≥1200 km from east to west between the Lhasa and Qiangtang blocks in central Tibet, includes Jurassic deep-sea turbidites, sedimentary mélange, and ophiolite remnants (DeCelles et al., 2007). Mid-Cretaceous to Cenozoic lacustrine and fluvial successions with interbedded volcanic rocks occur in the northern Nima and Lunpola basins (XZBGM, 1993; Kapp et al., 2005, 2007b).

The Qiangtang block, bounded to the south by the BNSZ and to the north by the Jinsha suture, is divided into the northern and southern Qiangtang terranes by an axial metamorphic belt including Triassic blueschist-bearing mélange (Pullen et al., 2008). In the southern Qiangtang terrane, Cambrian metasedimentary rocks intruded by Ordovician granites lie in tectonic contact with Carboniferous–Jurassic strata (Pullen et al., 2011). Jurassic sandstones and limestones were intruded in the Jurassic (150–170 Ma) and Cretaceous (100–130 Ma) by intermediate-felsic rocks yielding $\varepsilon_{Hf}(t)$ values ranging widely from –22 to +10 (Li et al., 2014b; Liu et al., 2017). Limited east-west–trending Cretaceous strata and non-marine Cenozoic deposits are exposed (XZBGM, 1993; Kapp et al., 2005).

Cretaceous Geology

The study area is located in the central and northern Lhasa terranes, where Early Cretaceous felsic andesites with minor basalts erupted between 143 and 102 Ma reach a thickness ≥1000 m and yield zircons with negative $\varepsilon_{Hf}(t)$ values (Zhu et al., 2011b). Lowermost Cretaceous shallow-marine to deltaic sandstone and shale interbedded with volcanic tuff (Zhang et al., 2011) are overlain by Aptian–Cenomanian limestones of the Langshan Formation, consisting of wackestone and packstone deposited in low-energy lagoonal to shallow reefal environments (Leier et al., 2007a; BouDagher-Fadel et al., 2017). The Late Cretaceous is represented by two non-marine clastic units—the Jingzhushan Formation in northern Lhasa, and the Daxiong Formation in central Lhasa—both unconformably overlain by Paleogene Linzizong volcanic rocks and continental red beds. In the southern Nima basin, strata equivalent to the Jingzhushan Formation are named "Upper Cretaceous Conglomerate unit" (Kuc unit of DeCelles et al., 2007 and Kcl unit of Kapp et al., 2007b).

The Jingzhushan Formation is exposed in a several-km-wide and >1000-km-long, east-west–trending belt along the northern perimeter of the Lhasa terrane from Biru in the east to Rutog in the west (Fig. 1B). The unit, unconformably overlying or in fault contact with Early Cretaceous strata in most areas, consists of conglomerate with minor red sandstone and siltstone (Pan et al., 2004; Volkmer et al., 2014). Depositional age was constrained by Late Cretaceous detrital-zircon ages and Aptian–Albian limestone clasts containing *Orbitolina* (Leier et al., 2007a; Volkmer et al., 2014). In section SE-N04 measured south of Dagze Co (Nima area; Fig. 1B), the Jingzhushan Formation overlies instead a ~500-m-thick, clast- or matrix-supported cobble to boulder volcaniclastic conglomerate (Kcv unit; Figs. 2 and 3) with a maximum depositional age of 97 ± 2 Ma (DeCelles et al., 2007; Kapp et al., 2007b). The broadly time-equivalent Daxiong Formation, exposed along a ~10-km-wide and ~700-km-long east-west–trending belt extending in the southern part of the central Lhasa terrane from the Coqen basin to the Nam Co (Fig. 1B; Pan et al., 2004), mostly consists of red volcaniclastic conglomerates. Based on three sections measured in the Coqen basin, its age was constrained as Cenomanian–Turonian (Sun et al., 2015a).

Cretaceous Tectonics

Cretaceous deformation in the central-northern Lhasa terranes is documented by doubly vergent east-west–striking thrusts (Fig. 1B). The Daxiong Formation was deposited along the front of the north-dipping Gugu La thrust (Fig. 1B), which carried Early Cretaceous volcanic rocks in its hanging wall and was active by 92 Ma, as documented by cross-cutting granite (Murphy et al., 1997). The coeval south-dipping Gaize-Siling Co thrust in the north carries Early Cretaceous strata in its hanging wall, with Late Cretaceous conglomerates deformed into a northward-verging overturned syncline in the proximal footwall (Kapp et al., 2007b; Volkmer et al., 2007; 2014). Crustal thickening and 46%–60% north-south shortening took place during the Cretaceous to Paleogene, as indicated by structural analysis and regional map-

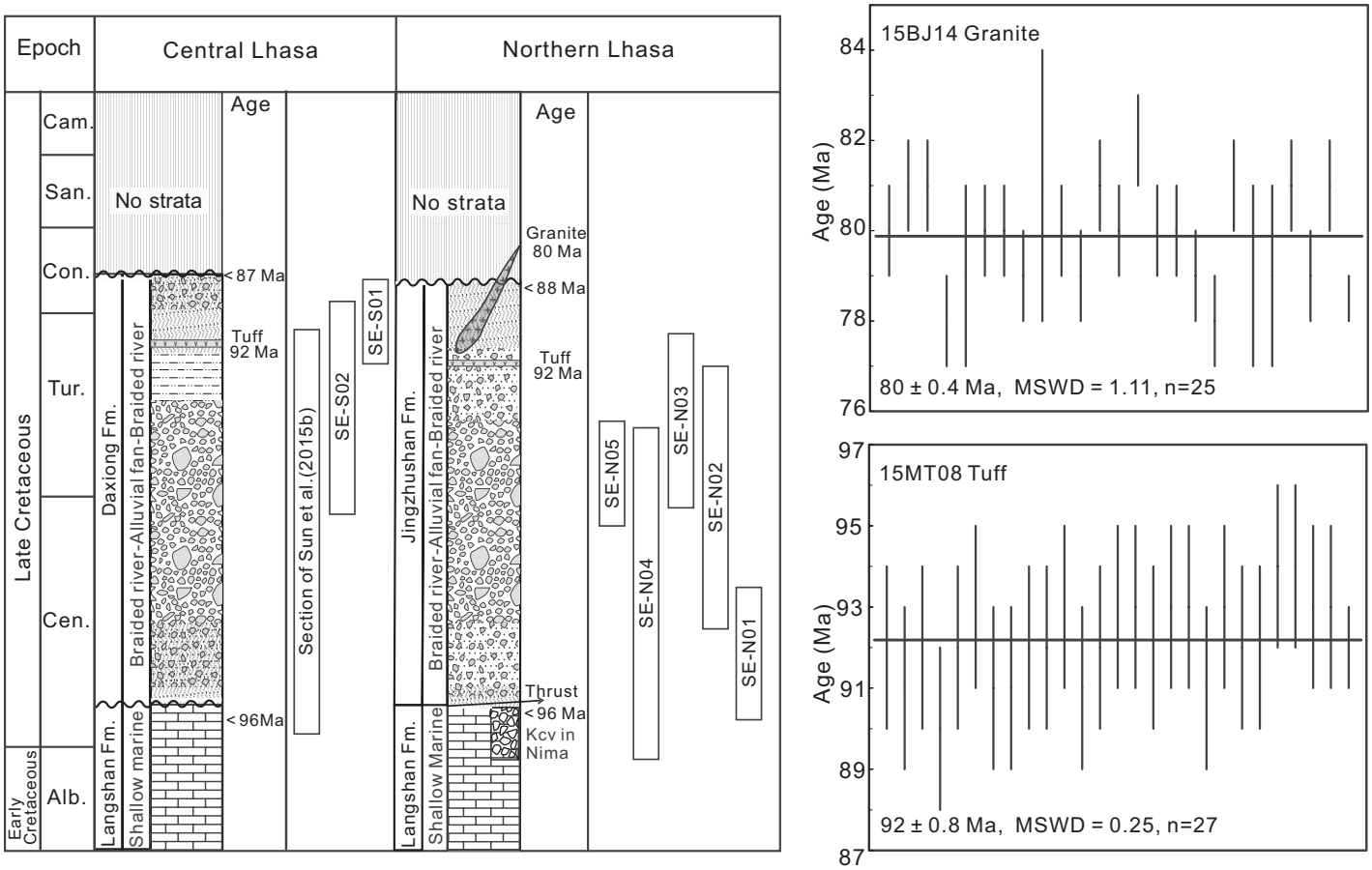

Figure 2. Comparison between Cretaceous strata in the central and northern Lhasa, Tibetan Plateau terranes. Lithological legend as in Figure 3, age of interbedded tuff layers from Daxiong as ca. 92 Ma is referred from Sun et al. (2015a). Fm.—Formation; Alb.—Albian; Cen.—Cenomanian; Tur.—Turonian; Con.—Coniacian; San.—Santonian; Cam.—Campanian; MSWD—mean square weighted deviation.

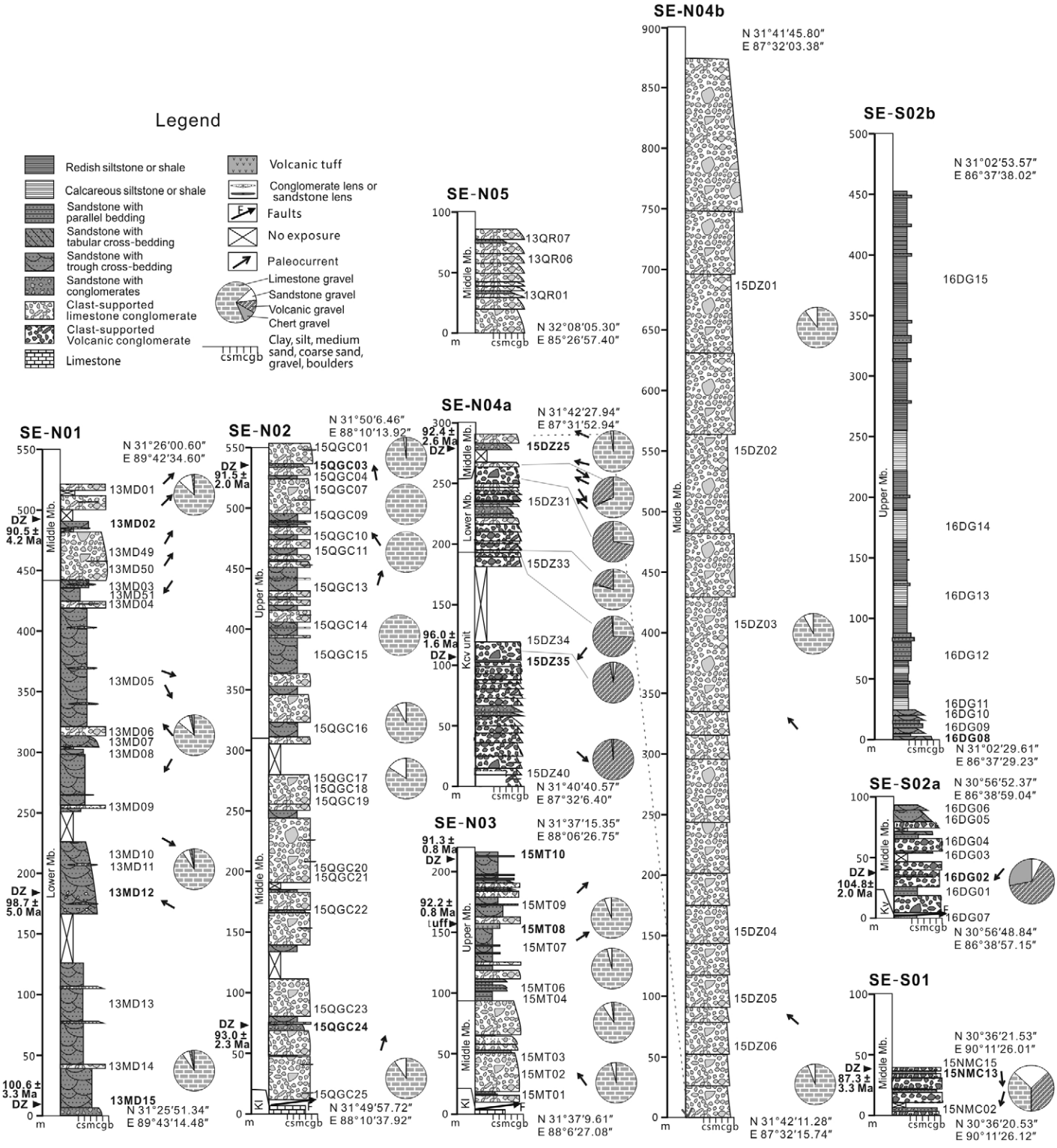

Figure 3. Stratigraphic columns of the Jingzhushan (SE-N01-05) and Daxiong formations (SE-S01-02) in the Lhasa block, Tibet, showing sample locations, gravel composition, and paleocurrent directions. Kl—mid-Cretaceous Langshan Formation limestone; Kv—Early Cretaceous volcanic rocks; Mb.—member; DZ—detrital zircon YC1σ (2+) ages (calculated after Dickinson and Gehrels 2009).

ping east of Nam Co (Kapp et al., 2007a) and in the Duba (Volkmer et al., 2014), Nima (Kapp et al., 2007b), Coqen (Murphy et al., 1997), Xiagangjiang (Volkmer et al., 2007), and Shiquanhe regions (Kapp et al., 2003).

METHODS

Sedimentology and Petrography

We measured stratigraphic sections at seven localities (sites shown in Fig. 1B), described sedimentary structures, and identified depositional environments by an investigation of lithofacies associations, following procedures outlined in Miall (1996). Paleocurrent directions were measured in the field from trough cross-strata in sandstone beds and from clast imbrication in conglomerate beds. Results were corrected to horizontal by standard stereonet techniques, and the average trough-axis orientation of each point was determined statistically on a stereographic plot of 15–20 trough limbs (method I of DeCelles et al., 1983).

The petrographic composition of nine sandstone samples from the Daxiong Formation and of 33 samples from the Jingzhushan Formation was determined by counting over 350 grains per thin section following the Gazzi-Dickinson method. Lithologies of conglomerate clasts were identified in the field, and 50 clasts or more were counted at each site using a 10x10 cm grid. About 1800 conglomerate clasts were counted overall in measured sections of the Kcv, Jingzhushan (27 sites), and Daxiong units (3 sites) (Fig. 3; Table DR3[1]).

Zircon Dating and Hf Isotopes

Zircons were separated from medium-grained sandstones, granite, and tuff. U-Pb dating was conducted by laser ablation–inductively coupled plasma–mass spectrometry at the State Key Laboratory of Mineral Deposits Research, Nanjing University, following Jackson et al. (2004). The interpretation of zircon ages is based on $^{206}Pb/^{238}U$ ages if <1000 Ma and on $^{207}Pb/^{206}Pb$ ages if >1000 Ma. Zircon grains with discordance <10% were considered valid. Age calculations and concordia diagrams were created using Isoplot 3.23. The maximum depositional age of strata, was calculated as the mean age of the youngest two or more grains overlapping in age at 1σ (YC1σ (2+) (Dickinson and Gehrels, 2009).

In situ Hf isotopic analyses on detrital zircons yielding U-Pb ages <250 Ma were conducted on the same spot as U-Pb analyses. Hf isotopic compositions were obtained with a Thermo Scientific Neptune Plus multicollector–inductively coupled plasma–mass spectrometer coupled with a New Wave UP193 solid-state laser ablation system at Nanjing University, China. Zircon grains were ablated with a beam diameter of 35 μm with an 8-Hz laser repetition rate, and with an energy of 15.5 J/cm^2. Results were calculated assuming 1.865×10^{-11} a^{-1} for the decay constant of ^{176}Lu.

Overall, we dated 670 detrital zircons in nine sandstone samples from the Jingzhushan Formation and 225 detrital zircons in three samples from the Daxiong Formation (sampling sites shown in Fig. 3); 863 concordant ages and 384 Hf isotopic values from zircons younger than 250 Ma were obtained (Tables DR5 and DR6 [see footnote 1]). The maximum depositional ages of 12 samples are shown in Table DR2 (see footnote 1) and Figure 3.

Kcv UNIT AND JINGZHUSHAN FORMATION

Sedimentology and Stratigraphy

Beds of the Kcv unit are up to 20 m thick and intercalated with minor lenses of coarse sandstone. Very poorly sorted conglomerates contain angular to subangular volcanic clasts, ranging in diameter from 1 to 20 cm (lithofacies Gcm and Gmm, terminology after Miall 1996; see details in Table DR1 [see footnote 1]). Clast imbrication in clast-supported conglomerate (Lithofacies Gch) indicates roughly southward paleocurrents. Deposition by viscous debris flows on a proximal fan fed by an elevated source area in the north is inferred (DeCelles et al., 2007).

The Jingzhushan Formation, separated from the underlying Langshan Formation by the Gaize-Siling Co thrust in sections SE-N02 and SE-N03, comprises red sandstone and conglomerate with fining-upward successions (Figs. 3, 4B, and 4C). Mottled conglomerate beds range between 2 and 5 m in thickness and may include lenses of coarse-grained sandstone (~20–50 cm). Fining-upward successions are up to 50 m thick. Clasts are angular to sub-rounded and are 10–30 cm in diameter, but may reach 1 m. Conglomerates are dominantly clast-supported, poorly sorted, and structureless (lithofacies Gcm), although cobble conglomerates may display crude horizontal laminae, graded bedding, or clast imbrication (Fig. 4F, lithofacies Gch). Matrix-supported and poorly sorted conglomerates (Fig. 4E, lithofacies Gmm) occur. Lenticular sandstones contain mainly planar or trough cross-stratification (lithofacies Sp or St).

Medium- to coarse-grained red sandstone beds, 30–200 cm thick and with sparse granules and pebbles at the base, show trough or planar cross-stratification (Fig. 4G, St and Sp) and pass upward into medium-grained sandstones with horizontal lamination and rare current ripples (lithofacies Sh). Red laminated siltstone or claystone may occur at the top of fining-upward sequences (Fig. 4H, lithofacies Fl). Several 20–50-cm-thick tuff beds are intercalated in section SE-N03 (Figs. 3 and 4H).

Paleocurrent directions obtained on trough cross-stratification and imbricated clasts indicate mostly northward paleoflow (Fig. 3); south-directed paleocurrent indicators were observed in sections SE-N01 and SE-N04 (Fig. 3).

Environmental Interpretation

Sedimentary features as described above allow us to subdivide the Jingzhushan Formation into a lower sandstone-conglomerate member, a middle conglomerate member, and an upper sandstone-conglomerate member (Figs. 3, 4A, and 4C). The Jingzhushan Formation is dominated by lithofacies Gcm, Gmm, Gch, St, and Sp with fine-grained sandstone and siltstone (Sh and Fl) occurring only in thin discontinuous interbeds. The individual lithofacies or association of different lithofacies indicate different depositional processes, as interpreted below.

The structureless fabric and poor sorting of matrix supported conglomerate with boulder-size clasts indicate that lithofacies Gcm and Gmm consist of rock-avalanche deposits formed by slope failure and accumulation close to paleorelief. The wide range of clast size, poorly organized texture, faint lamination, and imbrication of lithofacies Gch suggest rapid deposition from a highly concentrated sediment gravity flow (Blair and McPherson, 1994).

Interbedded lenticular sandstones (St and Sp) are interpreted as overbank deposits or waning stages of in-channel flows. Fining-upward sandstone packages less than 2 m thick and displaying trough or planar cross-stratification indicate deposition in shallow (<2 m deep) and unstable braided channels. Siltstones or mudrocks (F1) accumulated during waning overbank flow (Miall, 1996).

Collectively, these lithofacies and inferred depositional processes imply an alluvial-fan environment and gravelly braided channels adjacent to actively eroding highlands in the south. The coarsening- and thickening-upward megasequence including the lower and middle members (Figs. 2 and 3) indicates progradation from stream flows and distal alluvial-fan to proximal alluvial-fan settings. The fining- and thinning-upward trend displayed by the upper member (Figs. 2 and 3) indicates instead retrogradation and transition to distal alluvial-fan and braidplain environments.

[1]GSA Data Repository item 2019138, Figure DR1 and Tables DR1–DR6, is available at http://www.geosociety.org/datarepository/2019 or by request to editing@geosociety.org.

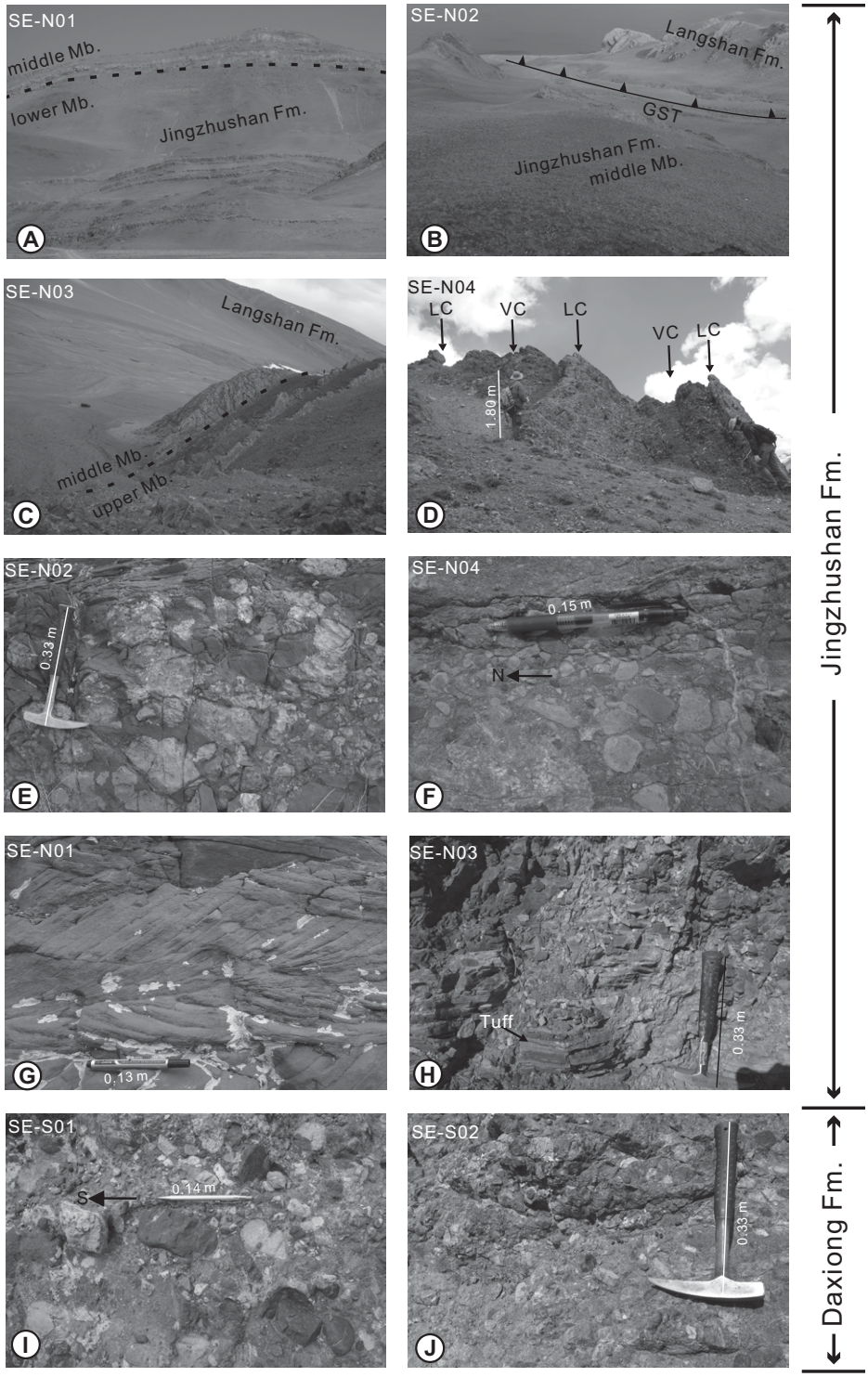

Figure 4. Field photographs of the Jingzhushan and Daxiong formations, Lhasa block, Tibet: (A) lower and middle members (section SE-N01, Duba); (B) middle and upper members, separated from the Langshan Formation by the Gaize-Siling Co thrust (SE-N02, Qiagui Co); (C) same units and thrust in section SE-N03 (Wuru Co area); (D) lower member with alternating conglomerates with volcanic-dominated (VC) and limestone-dominated clasts (LC) (SE-N04); (E) matrix-supported conglomerate (SE-N02); (F) imbricate clasts indicating northward paleoflow (SE-N04); (G) sandstone with cross-stratification (SE-N01); (H) tuff bed (SE-N03); (I) imbricate clasts indicating southward paleoflow (SE-S01); (J) conglomerate (SE-N02). Fm.—Formation; Mb.—Member; GST—Gaize-Siling Co thrust.

Age Constraints

The depositional age of the Jingzhushan Formation is constrained by the age of interbedded tuff layers, the youngest ages of detrital zircons, microfossils contained in limestone clasts, and the age of intrusive granite. Twenty-seven zircon grains contained in a tuff bed intercalated at the top of the middle member yield a single population with weighted average age 92 ± 0.8 Ma (Figs. 2 and 5D, sample 15MT08). From eastern to western sections, maximum depositional ages calculated for the Jingzhushan Formation are 91 ± 4 Ma (13MD02), 92 ± 2 (15QGC03), 91 ± 1 Ma (15MT10), 92 ± 3 Ma (15DZ25), and 90 ± 3 Ma (13QR01) (Fig. 3; Table DR2). Rose and Durant (2011) showed that fine-grained ash produced during even large eruptions takes only a few days to settle. These YC1σ (2+) ages thus provide firm chronostratigraphic evidence of synchronous deposition for the entire east-west–trending, >1000 km-long Jingzhushan conglomerate belt between 92 and 90 Ma.

In addition, the youngest detrital zircons from the top of the underlying Kcv unit fix its maximum depositional age of 96 ± 2 Ma (15DZ35). Granite intruded into the Jingzhushan Formation is dated as 80 ± 0.4 Ma (Fig. 2, 15BJ14). Limestone clasts from the Jingzhushan Formation yielded planktonic foraminifera, including *Helvetoglobotruncana praehelvetica* (Fig. DR1i; see footnote 1), *Whiteinella archaeocretacea* (Fig. DR1j), *Whiteinella sp.* (Fig. DR1k), and poorly preserved *Thalmanninella greenhornensis* (Fig. DR1l), suggesting a late Cenomanian to earliest Turonian age (ca. 95–93 Ma; BouDagher-Fadel, 2015) for carbonate rocks in the source area. Collectively, these data indicate that the Kcv unit was deposited in the latest Cenomanian (i.e., post 96 Ma), and was overlain by the Jingzhushan Formation deposited during the Turonian (ca. 92 Ma), after the Cenomanian (post-95–93 Ma) and before the late Campanian (80 Ma).

Conglomerate and Sandstone Petrography

Conglomerate clasts in the Kcv unit are dominantly volcanic (>95%), with minor sandstone and chert. Either volcanic (20%–73%) or Langshan limestone clasts (25%–79%) are dominant at the base of the Jingzhushan Formation in section SE-N04a (Figs. 3 and 4D). The middle and upper members of the Jingzhushan Formation are characterized by *Orbitolina*-rich limestone clasts (>84%), associated with sandstone-siltstone (2%–16%), and rare chert (Figs. 3, 4E, and 4F).

Twenty-eight sandstone samples from five measured sections of the Jingzhushan Formation are mostly quartzo-lithic and subordinately litho-

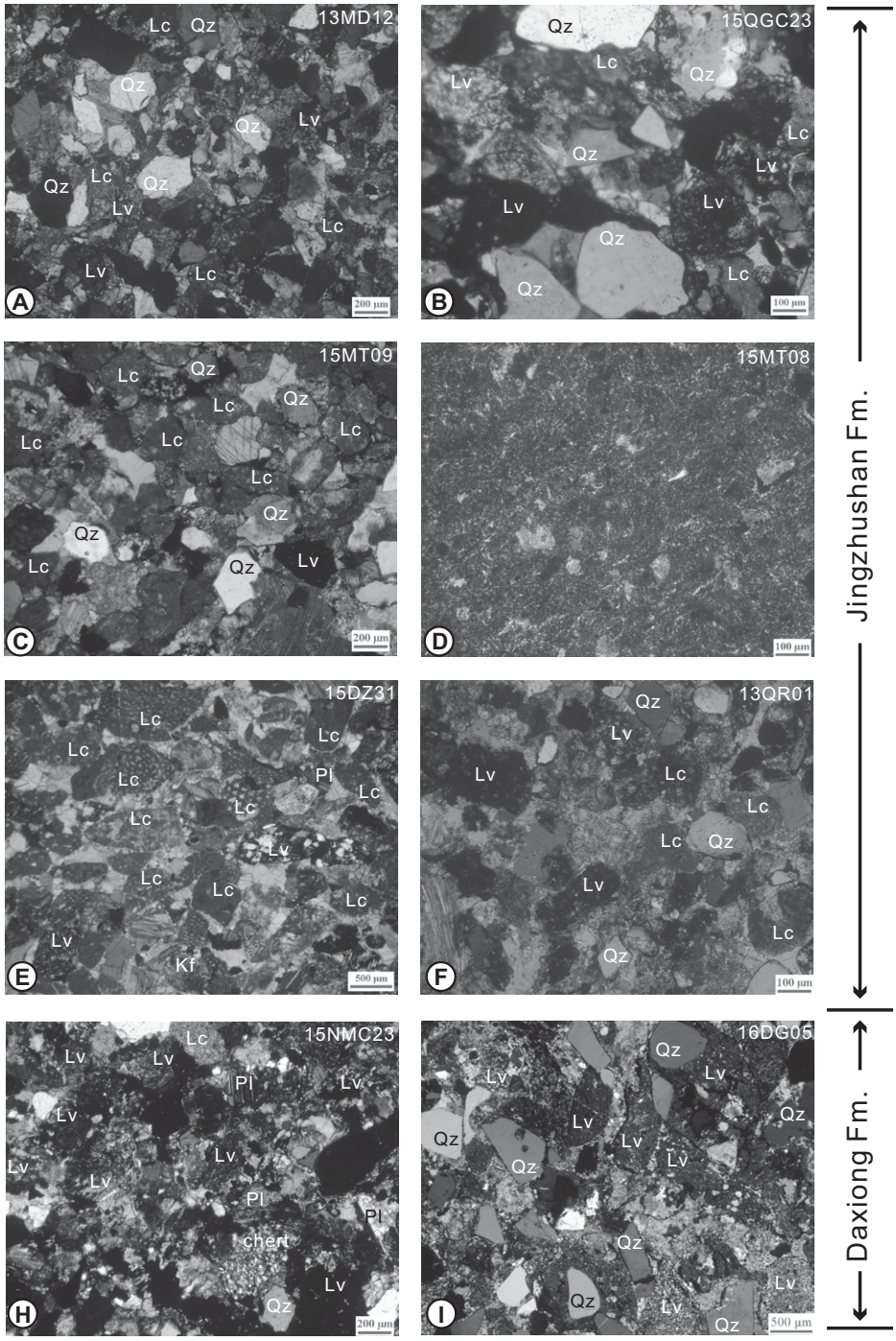

Figure 5. Sandstone petrography of the Jingzhushan and Daxiong formations, Lhasa block, Tibet: (A) quartzo-lithic sandstone (13MD12, section SE-N01); (B) quartzo-lithic volcaniclastic sandstone (15QGC23, SE-N02); (C) quartzo-lithic carbonaticlastic sandstone (15MT09, SE-N03); (D) tuff (15MT08, SE-N03); (E) lithic carbonaticlastic sandstone (15DZ31, SE-N04); (F) lithic sandstone (13QR01, SE-N05); (G) lithic volcaniclastic sandstone (15NMC23, SE-S01); (H) quartzo-lithic volcaniclastic sandstone (16DG05, SE-S02). Qz—quartz; Pl—plagioclase; Lv—volcanic lithic; Lc—carbonate lithic.

quartzose and lithic (average modal composition Q:F:L = 28:2:70; Table DR4 [see footnote 1]; Figs. 5A–5C, 5E, 5F, and 6A). Grains are poorly sorted, angular to sub-rounded, and calcite-cemented. Monocrystalline quartz represents only 1%–4% of framework grains at the base of the Jingzhushan Formation in section SE-N04, and increases to 16%–25% in the middle and upper members in sections SE-N02, N03, and N05, reaching a maximum (28%–59%) in section SE-N01. Lithic grains (40%–96%) are mainly felsic/intermediate volcanic types (43% of total lithics on average) and limestone (56% of total lithics); chert, mafic-igneous and metamorphic rock fragments are rare (Fig. 6B).

Detrital Zircon U-Pb Ages and Hf Isotopes

In the Kcv unit, 73 concordant ages were obtained from sample 15DZ35 (section SE-N04, south of Dagze Co, Nima area; Figs. 1B and 3). Among these, 64 cluster between 90 and 120 Ma (peak at 105 Ma), and have εHf(t) values between +7.4 and +14.4 with T^{C}_{DM} model ages between 0.25 and 0.69 Ga (Figs. 7 and 8; Tables DR5 and DR6).

In the Jingzhushan Formation (Figs. 7 and 8; Tables DR5 and DR6), samples 13MD02, 13MD12, and 13MD15 (section SE-N01, Duba area; Figs. 1B and 3) yielded 194 concordant ages, 126 of which cluster between 90 and 150 Ma (peak at ca. 120 Ma). Seventy-seven Mesozoic zircons yielded εHf(t) values between –24.1 and +7.4, with T^{C}_{DM} model ages between 0.71 and 2.73 Ga. Older U-Pb ages cluster in the 250–350, 400–650, 700–950, 1000–1200, 1800–1950, and 2250–2600 Ma age ranges.

Sample 15QGC03 and 15QGC24 (section SE-N02, north of Qiagui Co; Figs. 7 and 8) yielded 145 concordant ages, 97 of which cluster between 90 and 150 Ma (peaks at 97 and ca. 120 Ma), 75 Mesozoic zircons yielded εHf(t) values between –16.2 and +15.31, with T^{C}_{DM} model ages between 0.18 and 2.28 Ga. Older U-Pb ages cluster in the 250–350, 450–500, 700–950, 1000–1250, and 1800–2000 Ma age ranges.

Out of the 93 concordant ages obtained from section SE-N03 (south of Wuru Co; Figs. 7 and 8), 73% are younger than 250 Ma. Forty-eight Mesozoic zircons have cluster between 90 and 120 Ma (peaks at 95 and ca. 110 Ma), yielded εHf(t) values between –11.4 and +11.8, with T^{C}_{DM} model ages between 0.40 and 1.89 Ga. The complex age spectrum includes clusters at 90–120, 250–300, 300–600, 900–1100, and 1850–2050 Ma.

Sample 15DZ25 (section SE-N04, south of Dagze Co, Nima area; Figs. 7 and 8) yielded 72 concordant ages, 42 of which have cluster between 90 and 140 Ma (peaks at ca. 92, ca. 103, and ca. 123 Ma). Thirty Mesozoic zircons yielded εHf(t) values between –18.6 and +14.7, with T^{C}_{DM} model ages between 0.22 and 2.38 Ga. Older U-Pb ages cluster in the 250–350, 350–500, 750–900, 1050–1150, and 1700–2000 Ma age ranges.

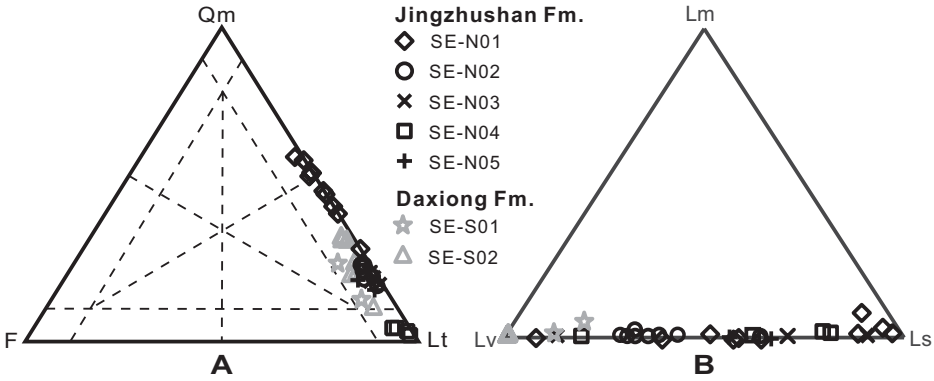

Figure 6. Petrographic plots of the Jingzhushan and Daxiong formations, Lhasa block, Tibet. Qm—monocrystalline quartz. F—feldspar; Lt—total lithic grains; Lv—volcanic; Ls—sedimentary; Lm—metamorphic; Fm.—Formation. Fields after Garzanti (2016).

Sample 13QR01 (section SE-N05, south of Zhaxi Co, Gaize area; Figs. 7 and 8) yielded 66 concordant ages, out of which 28 are between 90 and 160 Ma (peaks at ca. 92, ca. 103, ca. 126, and ca. 142 Ma). Twenty-six Mesozoic zircons yielded εHf(t) values between –12.0 and +19.4, with T_{DM}^{C} model ages between 0.04 and 2.02 Ga. Older U-Pb ages cluster in the 250–300, 450–500, 700–1000, 1050–1200, 1250–1350, and 1650–1850 Ma age ranges.

Provenance Interpretation

In the Kvc unit (section SE-N04), imbricated conglomerate clasts indicate mostly southward direction of sediment transport. Age spectra and isotopic signatures of detrital zircons (cluster at 90–120 Ma with peak at ca. 105 Ma; 23 of 27 grains with positive εHf(t) values between 7.4 and 12.0) match those from Early Cretaceous volcanic rocks in the BNSZ (Liu et al., 2017), indicating provenance from the north.

In the Jingzhushan Formation, the lack of detrital zircons in the 190–220 Ma age range, characteristic of the southern Qiangtang terrane, and of clasts derived from turbiditic sandstones and ophiolites exposed along the BNSZ in the north, rule out these two potential northern sources (Fig. 7). Sedimentary facies of the Jingzhushan Formation suggest limited transport distance (Fig. 3; <15 km; Blair and McPherson, 1994) and deposition in alluvial-fan to braided-river systems. Detrital zircons with negative εHf(t) values were not derived from the Gangdese arc in the southern Lhasa terrane, which is characterized by high positive εHf(t) values (Fig. 8; Ji et al., 2009; Zhu et al., 2011b). Conversely, the small amount of detrital zircons with εHf(t) >10 may have been derived from the Gangdese arc as air-fall ash. The Lhasa block is proposed to have had a width of ~600 km before 50% crustal shortening took place in the Cretaceous–Cenozoic time interval (Fig. 9; Murphy et al., 1997; Kapp et al., 2007a; 2007b; Volkmer et al., 2007; 2014), but it is well known that ash can travel by air for 1000 km or more, as documented for the 1980 Mount St. Helens, Washington, USA eruption (Sarna-Wojcicki et al., 1981).

A southern source for the conglomerates in the Jingzhushan Formation is suggested by clast imbrication indicating northward paleoflow and by the abundance of *Orbitolina*-bearing clasts identical to marine limestones of the Langshan Formation exposed in the central and northern Lhasa terranes (Fig. DR1; BouDagher-Fadel et al., 2017). Moreover, detrital zircons yielding ages of 90–150 Ma and widely ranging εHf(t) values, or clustering between 1000 and 1300 Ma (Figs. 7 and 8), match those from Late Paleozoic strata (Leier et al., 2007b; Zhu et al., 2011a), Cretaceous igneous rocks, and clastic sediments of the central and northern Lhasa terranes (Zhang et al., 2011; Zhu et al., 2011b).

A provenance change from the Kcv unit to the overlying Jingzhushan Formation is documented by the 180° change in paleocurrent directions and different clast composition (Figs. 3 and 4D). Contrary to the Kvc unit, the Jingzhushan Formation was fed from the south, where mid-Cretaceous limestones of the Langshan Formation and Early Cretaceous volcaniclastic sandstones of the Duoni Formation were exposed to erosion.

DAXIONG FORMATION

Stratigraphy and Sedimentology

The Daxiong Formation is at least 550 m thick in section SE-S02 (Tangra Yum Co area), whereas only ~45-m-thick conglomerates are exposed in section SE-S01 (Nam Co area) (Fig. 3).

Red pebble to cobble conglomerate beds are characterized by lithofacies Gcm and Gch in sections SE-S01 and SE-S02a. Unsorted clasts are subangular to subrounded, and range mostly from 2 to 10 cm in diameter but locally exceed 40 cm. Medium- to coarse-grained sandstone beds, with horizontal planar lamination or trough cross-stratification (Sh and St; Table DR1) occur at the top of conglomerate beds.

In the lower part of section SE-S02b, fine- to medium-grained sandstones show climbing-ripple lamination, horizontal lamination, or trough cross-stratification (lithofacies Sh, Sr, and St; Table DR1). The upper part is characterized by monotonous red and yellow siltstone locally yielding fossil plants (Fr); minor sandstone lenses ~50 cm thick and with ripples and horizontal lamination are intercalated (Sh).

Environmental Interpretation

The conglomeratic lithofacies Gcm and Gch with minor Sh interbeds exposed in the Nam Co and Tangra Yum Co areas indicate deposition by clast-rich debris flows (Blair and McPherson, 1994). The sandy lithofacies Sh and St in the Tangra Yum Co area were deposited in braided-river channels (Miall, 1996). Monotonous fine-grained sequences (e.g., Fr) in the upper part, are interpreted as floodplain deposits. The discontinuous lenses of fine sandstone (Sh, Sr, and St) represented crevasse-splay deposits or migrating stream-flow channels (Miall, 1996).

Sedimentary features of the Daxiong Formation indicate deposition in alluvial-fan and braided-river environments, similarly to the Daxiong Formation in the Coqen basin (Sun et al., 2015a), and also to the Jingzhushan Formation.

Age Constraints

The Daxiong Formation lacks fossils and interbedded tuffs. Its maximum depositional age is constrained by the youngest detrital zircons (Table DR2), dated as 94 ± 2 Ma in the Tangra Yum Co area (16DG08) and as 87 ± 3 Ma in the Nam Co area (15NMC13, shown in Table DR2 and Fig. 3). According to Sun et al. (2015a), the Daxiong Formation in the Coqen basin was deposited between the early Cenomanian (ca. 96 Ma) and the Turonian (ca. 92 Ma), with interbedded tuff layers dated as ca. 92 Ma. Deposition of the Daxiong Formation was therefore approximately coeval with the Jingzhushan Formation, and was deposited between <96 Ma to ca. 92 Ma and until ca. 87 Ma.

Conglomerate and Sandstone Petrography

In section SE-S02 (Tangra Yum Co area), volcanic rocks represent 65% of total clasts from the conglomerate in the Daxiong Formation, with 7% quartzose sandstone, and 28%

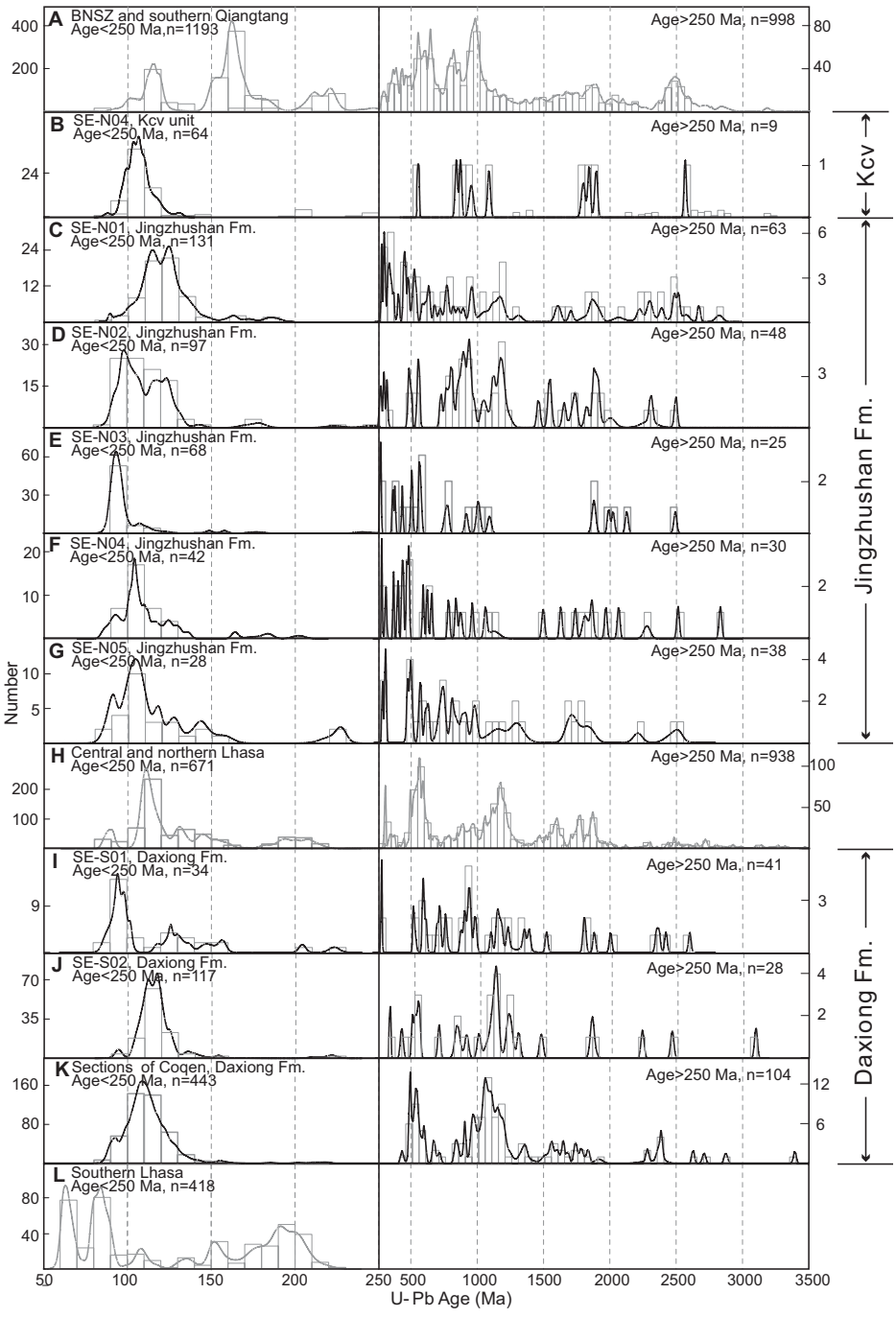

Figure 7. Relative U-Pb age probability for detrital zircons from Jingzhushan sandstones (C–G; sections SE-N01 to N05), Kcv sandstones (B; section SE-N04), and Daxiong sandstones (I–K; sections SE-S01-02 and Coqen basin; Sun et al., 2015b), in Lhasa block, Tibet. Results are compared with data from: (A) detrital and igneous zircons in the southern Qiangtang and Bangong-Nujiang suture zone (BNSZ) (Kapp et al., 2007b; Pullen et al., 2008; Gehrels et al., 2011; Zhu et al., 2011a, 2011b; Li et al., 2014b; Liu et al., 2017), (H) detrital and igneous zircons from central-northern Lhasa (Chu et al., 2006; Leier et al., 2007a; Gehrels et al., 2011; Zhang et al., 2011; Zhu et al., 2011a, 2011b; Sun et al., 2015b), and (L) igneous zircons from southern Lhasa (Chu et al., 2006; Ji et al., 2009; Zhu et al., 2011b). Fm.—Formation.

chert. Similar proportions were observed in the Coqen basin (Sun et al., 2015a). In section SE-S01 (Nam Co area), clasts are mostly volcanic (35%–42%), sedimentary sandstone (15%–24%), and metamorphic limestone (35%–40%), with minor chert (Figs. 3, 4I, and 4J).

Sandstones in the Daxiong Formation are poorly sorted with mostly angular to subrounded grains (Figs. 5G and 5H). Nine samples from two sections are quartzo-lithic (average modal composition Qt:F:L = 24:4:72; Table DR4; Fig. 6A) with mainly felsitic and subordinately microlitic volcanic fragments. Quartz is mostly monocrystalline and occasionally well rounded (Fig. 6B).

Detrital Zircon U-Pb Ages and Hf Isotopes

Zircon grains from sample 15NMC13 (section SE-S01, northwest of Nam Co; Figs. 7 and 8) yielded 28 out of 75 valid ages in the 90–160 Ma range (peaks at ca. 93 and ca. 125 Ma). Thirty-one zircon grains of Mesozoic age yielded εHf(t) values between –10.4 and +10.5, with T_{DM}^{C} model ages between 0.54 and 1.79 Ga (Table DR6; Fig. 8). Older U-Pb ages cluster in the 500–600, 450–500, 700–1000, 1050–1200, 1300–1400, and 1800–2500 Ma age ranges (Table DR5; Fig. 7).

Zircon-age spectra from samples 16DG02 and 16DG08 (section SE-S02, east of Tangra Yum Co; Figs. 7 and 8) are similar. Out of 135 valid ages, 117 cluster between 90 and 140 Ma (peaks at ca. 94 and ca. 115 Ma). Twenty-six zircon grains with Mesozoic age yielded εHf(t) values between –12.6 and +9.1, with T_{DM}^{C} model ages between 0.58 and 1.99 Ga (Table DR6; Fig. 8). Older U-Pb ages cluster in the 450–500 and 1050–1300 Ma age ranges (Table DR5; Fig. 7).

Provenance Interpretation

The lack of detrital zircons with εHf(t) values >10 rule out provenance from the Gangdese arc in the southern Lhasa terrane, and rather indicates a northern source. The BNSZ and southern Qiangtang terrane have similar zircon age patterns (cluster at ca. 110 Ma) and εHf(t) values. However, they are unlikely sources because during the Late Cretaceous elevated central-northern Lhasa terranes were supplying detritus to the Jingzhushan Formation south of the BNSZ (DeCelles et al., 2007 and this study). A more proximal source within central-northern Lhasa, specifically including Early Cretaceous volcanic rocks exposed in the north, is indicated by southward paleocurrent directions and abundance of felsitic and microlitic volcanic grains. Marble clasts and Mesoproterozoic zircons (1000–1300 Ma, peak at ca. 1150 Ma) with ages matching those from Late Paleozoic strata of the central and northern Lhasa terranes (Leier et al., 2007b; Gehrels et al., 2011; Zhu et al., 2011a) suggest additional contributions from underlying Paleozoic strata.

DISCUSSION

Growth of the Northern Lhasaplano

During the late Cenomanian to early Turonian, widely considered as a period of global sea-level rise (Haq, 2014), shallow marine carbonate deposition (Langshan Formation) in the central-northern Lhasa terranes, was replaced by continental Jingzhushan conglomerates (Figs. 3 and 10). Disappearance of marine seaways during a time of sea level rise implies surface uplift at that time.

The provenance change from the already terrestrial Kcv unit to the Jingzhushan Formation, associated with a 180° change in paleocurrent directions and markedly different clast composition (Figs. 3 and 4D), also indicates the development of topography south of the Jingzhushan Formation between 96 and 92 Ma.

Both Jingzhushan and Daxiong formations (Figs. 1B and 2) are characterized by middle alluvial fan to braidplain environments passing upward to proximal alluvial fans and finally braided rivers. Deposition must have taken place close to the source, with gravel size and strata thickness increasing first and decreasing next. For both formations, mainly deposited during the Turonian, provenance analysis suggests supply from the central-northern Lhasa terranes via north-directed and south-directed short and steep drainage systems (Fig. 10B). The northern part of the central Lhasa terrane and the southern part of the northern Lhasa terranes thus ceased to be a basin at the close of the Early Cretaceous, when they were uplifted to become a major source of detritus.

Such an early stage of plateau uplift is independently supported by pieces of geological evidence other than the sedimentary record. Post-Cenomanian tectonic activity is documented by northward motion along the Gaize-Siling Co thrust, which carried Langshan limestones in the hanging wall while the Jingzhushan Formation was being deposited in its footwall (Kapp et al., 2007b). At the same time, Cretaceous strata were carried southward along the Gugu La thrust while the Daxiong Formation was being deposited in its footwall (Murphy et al., 1997; Pan et al., 2004). Structural restorations document more than 50% crustal shortening across the Lhasa block since the early Late Cretaceous (Fig. 9). Penecontemporaneous Mg-rich and adakitic magmatism in the Lhasa block points to thickening and anatexis of a juvenile lower crust at the same time (Fig. 9; Sun et al., 2015a, and references therein). Tectonic and magmatic evidence are thus consistent with sedimentological and provenance analyses, indicating that a vast area, named the Northern Lhasaplano, started to grow and to be rapidly unroofed in the central-northern Lhasa terranes during the early Late Cretaceous (Fig. 10).

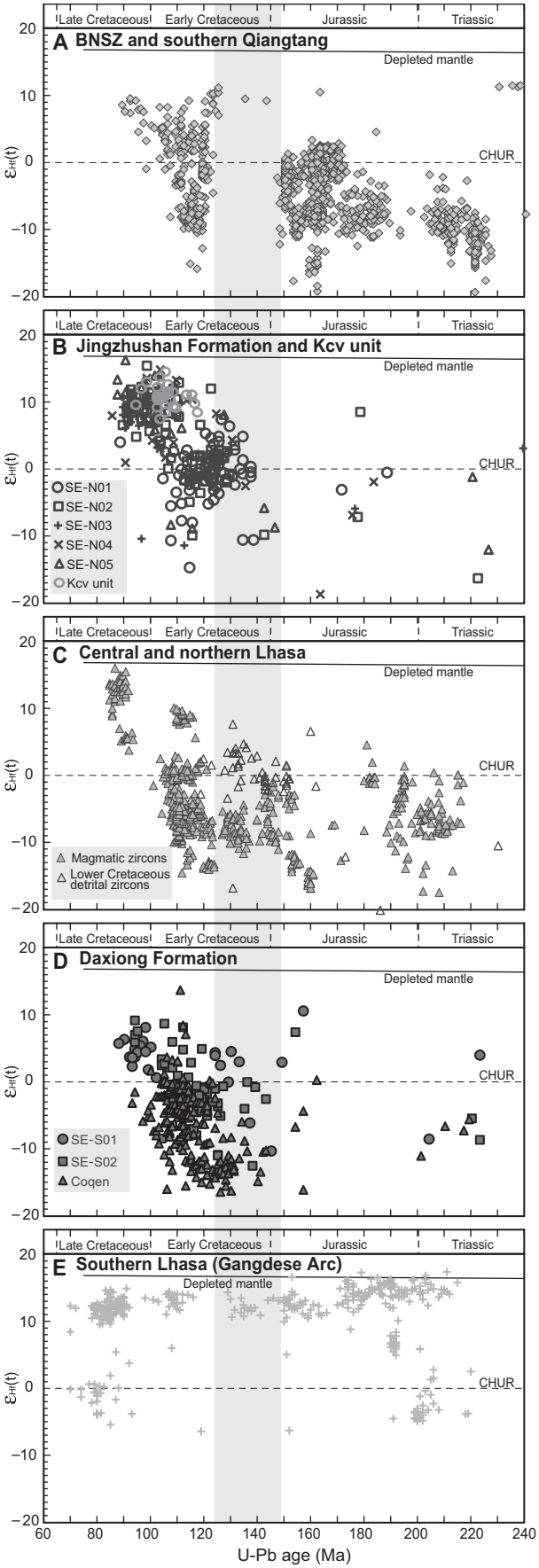

Figure 8. Age and Hf isotope signatures of detrital zircons from Jingzhushan sandstones (sections SE-N01 to N05), Kcv sandstones (section SE-N04), and Daxiong sandstones (sections SE-S01-02, and Coqen basin [Sun et al., 2015b]), in Lhasa block, Tibet. Results are compared with data from southern Qiangtang and Bangong-Nujiang suture zone (BNSZ) (Zhu et al., 2011b; Li et al., 2014b; Liu et al., 2017), igneous zircons from central-northern Lhasa (Chu et al., 2006; Zhu et al., 2011a; Sun et al., 2015a), detrital zircons from the Early Cretaceous sandstone in northern Lhasa (Table DR6; see footnote 1), and igneous zircons from southern Lhasa (Chu et al., 2006; Ji et al., 2009; Zhu et al., 2011b). CHUR—chondritic uniform reservoir.

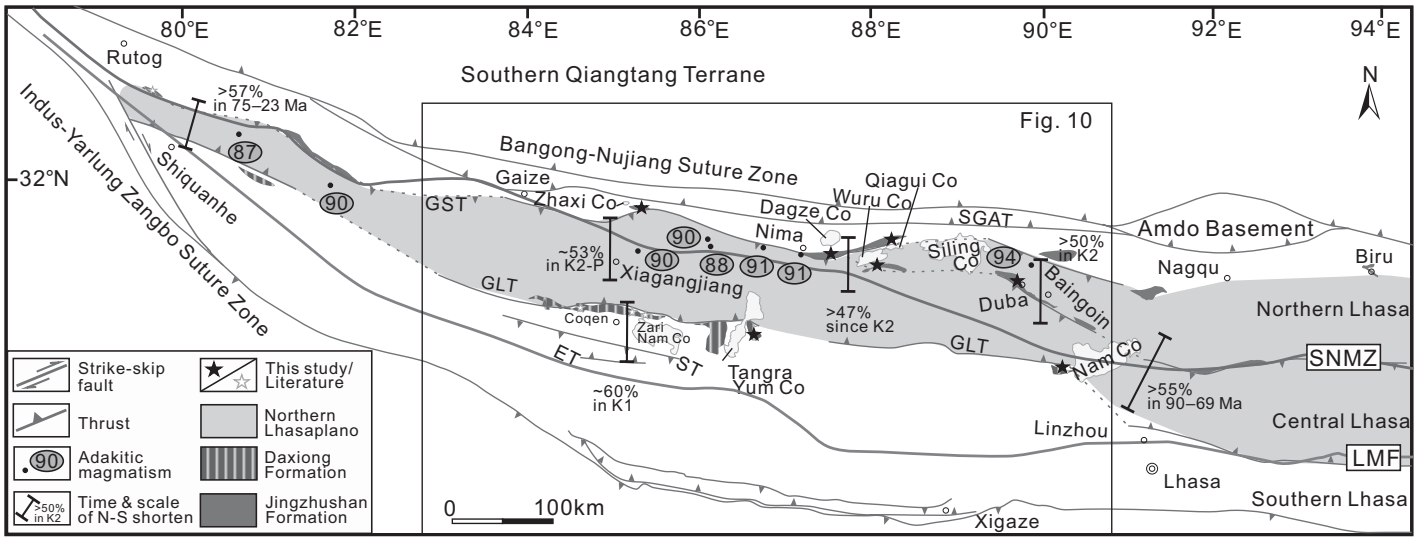

Figure 9. Simplified map indicating the location of the Northern Lhasaplano, together with the estimated N-S tectonic shortening (Murphy et al., 1997; Kapp et al., 2003, 2007a, 2007b; Volkmer et al., 2007, 2014) and the age of Late Cretaceous adakitic magmatism in central-northern Lhasa (Sun et al., 2015a and references therein). K1—Early Cretaceous; K2—Late Cretaceous; P—Paleogene; SGAT—Shiquanhe-Gaize-Amdo thrust belt; ET—Emei La thrust; ST—Shibaluo thrust; GLT—Gugu La thrust; GST—Gaize-Siling Co thrust; SNMZ—Shiquanhe-Nam Co Mélange zone; LMF—Luobadui-Milashan Fault.

Width of the Northern Lhasaplano

Synorogenic conglomerates are useful paleogeographic indicators of fault-bounded uplifts. The long and narrow belts of alluvial-fan conglomerates, deposited in the central-northern Lhasa terranes on the opposite sides of an area lacking Late Cretaceous–Paleogene strata (XZBGM, 1993), confine the northern and southern margins of the tectonically uplifted Northern Lhasaplano between the Gaize-Siling Co thrust in the north and the Gugu La thrust in the south (Fig. 1B). The northern front of the Northern Lhasaplano was over 1000 km long, from Rutog in the west (Li et al., 2014a) to Biru in the east (XZBGM, 1993) (Fig. 9). Its southern front extended for ~700 km from the Coqen basin (Sun et al., 2015a) to west of Nam Co (Fig. 9).

The Jingzhushan and Daxiong conglomerate belts lie today 80–150 km apart, indicating a minimum area of 80,000 km^2 for the Late Cretaceous Northern Lhasaplano (Fig. 9). If we consider subsequent upper crustal shortening >50% (Fig. 9), then the Northern Lhasaplano should have been >160 km wide and covered an area >160,000 km^2.

Evidence for the Timing of Initial Surface Uplift

There are several previous studies that help us to constrain further the timing of topographic uplift. Moderate cooling and exhumation of the Northern Lhasaplano was under way by 85 Ma (Rohrmann et al., 2012), providing a minimum age for onset of surface uplift. Thickening of the lower crust, indicated by high-Mg adakitic magmatism took place between 94 and 87 Ma beneath the Northern Lhasaplano (Fig. 9; Sun et al., 2015a and references therein). Numerous studies have suggested tectonic shortening across the Lhasa terrane by >50% began after the deposition of the Langshan Formation (Kapp et al., 2003, 2007a, 2007b; Volkmer et al., 2007, 2014).

Based on our observations, widespread deposition of *Orbitolina*-rich Langshan limestones on the northern Lhasa terrane continued until the latest Cenomanian to earliest Turonian (95–93 Ma), At ca. 92 Ma, the unconformably overlying Jingzhushan Formation containing *Orbitolina*-limestone clasts began to be deposited. This is compelling evidence of disappearance of marine seaways and onset of surface uplift and erosional exhumation between 93 and 92 Ma. Furthermore, fundamental information is provided by U-Pb dating of zircon crystals in tuffs interlayered within both Jingzhushan and Daxiong formations. The deposited age (ca. 92 Ma) of both Jingzhushan and Daxiong formations precisely constrains the timing of conglomerate deposition along both the northern and southern boundaries of the Northern Lhasaplano, and thus its initial topographic growth and erosion. The ca. 92 Ma age for onset of topographic growth is consistent with the evidence mentioned above, as well as with the activity of the Gaize-Siling Co and Gugu La thrusts. Stratigraphic, sedimentological, petrographic, geochronological, thermochronological, structural, and magmatic evidence thus concur to indicate that topographic growth of the Northern Lhasaplano began around 92 Ma, more than 30 Ma earlier than the onset of the India-Asia collision (assessed as 59 ± 1 Ma; Hu et al., 2015).

Implications for the Tectonic Evolution of the Tibetan Plateau

Reconstructing the tectonic evolution of the Northern Lhasaplano is essential to unravelling the subsequent paleogeographic evolution of the Tibetan Plateau. As Wang et al. (2014) summarized, early studies ascribed plateau uplift to continuous thickening and viscous flow of the underlying lithosphere without considering evidence for the timing of surface uplift. Based on the petrogenesis of K-rich magmatic rocks Chung et al. (1998) suggested that surface uplift did not occur before 40 Ma in the east and before 20 Ma in the west. Instead, paleoaltimetry studies based on oxygen isotopes favored northward growth of the plateau from Lhasa to Qiangtang during the Cenozoic (Rowley and Currie, 2006). Based on tectonic and paleoelevation evidence, Wang et al. (2008) suggested that an elevated proto-plateau existed already in the late Paleogene (ca. 40 Ma), and then surface uplift progressed both northward and southward. How, when and why topographic growth took place remained poorly constrained.

Early Cretaceous non-marine strata exposed along the BNSZ, together with provenance analysis in the northern Lhasa terrane have suggested uplift and erosion of the BNSZ in the

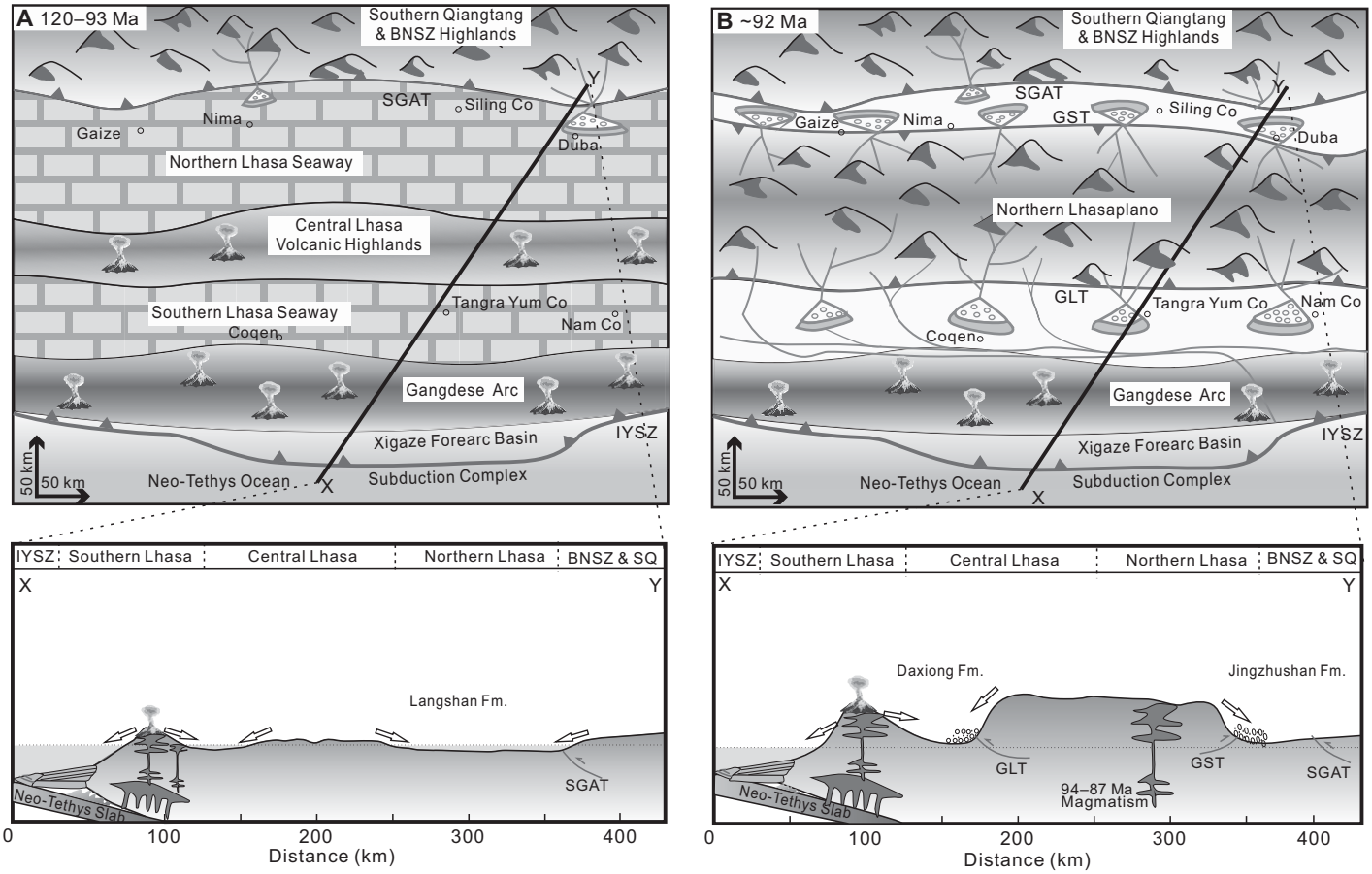

Figure 10. Paleogeographic and paleogeomorphological cartoons of the Lhasa block, Tibetan Plateau, in the Cretaceous (not to scale). (A) Aptian–Cenomanian (120–93 Ma): most of the area is occupied by a shallow epicontinental sea dominated by carbonate sedimentation (Leier et al., 2007a; Zhang et al., 2011; An et al., 2014). Tectonic uplift and exhumation affected parts of central Lhasa (e.g., Damxung area; Wang et al., 2017). The Xigaze forearc basin along the southern edge of the Lhasa block was being filled by deep-water turbidites (An et al., 2014). (B) Early Turonian (ca. 92 Ma): rapid uplift of the Northern Lhasaplano triggered erosion and accumulation of alluvial-fan conglomerates along its northern and southern flanks. BNSZ—Bangong-Nujiang suture zone; SQ—southern Qiangtang; GST—Gaize-Siling Co thrust; GLT—Gugu La thrust; IYSZ—Indus-Yarlung Zangbo Suture zone; SGAT—Shiquanhe-Gaize-Amdo thrust belt; Fm.—Formation.

Aptian–Cenomanian (DeCelles et al., 2007; Leier et al., 2007a; Ma et al., 2018). At this time, most of the Lhasa block was occupied by a shallow epicontinental sea with carbonate sedimentation (Fig. 10A; Zhang et al., 2011; Sun et al., 2017). Topographic growth in parts of the central Lhasa terrane began in the earliest Albian (e.g., Damxung area; Wang et al., 2017), where rapid erosional exhumation started to feed the Xigaze forearc basin at the southern edge of the southern Lhasa terrane (An et al., 2014; Orme and Laskowski, 2016).

Deposition of the Jingzhushan and Daxiong alluvial conglomerate belts, documenting retreat of the seaway and provenance of detritus from the Northern Lhasaplano took place around 92 Ma. Widespread high-Mg adakitic magmatism between 94 and 87 Ma indicates penecontemporaneous crustal thickening to ~50 km (Fig. 10B; Sun et al., 2015a and references therein).

Significant crustal thickening of the southern Lhasa terrane, instead, did not occur before 70 Ma (Zhu et al., 2017), and the central Lhasa terrane started to supply sediments to the shelved Xigaze forearc basin around 88 Ma (An et al., 2014). The Lhasa block, therefore, appears to have been raised in successive steps, first in the north and next in the south. Fold-thrust deformation initiated along the BNSZ in the north during the Early Cretaceous, and propagated southward with time (Kapp et al., 2007b), inducing tectonic inversion of sedimentary basins and initial growth of the Northern Lhasaplano between the Gaize-Siling Co and Gugu La thrusts in the early Late Cretaceous. The southern Qiangtang terrane and the BNSZ were uplifted notably earlier than the Northern Lhasaplano, thus initiating a topographic wave that swept stepwise southward across the Lhasa block during the Cretaceous.

The Andean-Style Tibetan Plateau in the Late Cretaceous

Pre-collisional growth of a proto-Tibetan plateau during an Andean-style orogeny has been a long-standing proposal (England and Searle, 1986; Kapp et al., 2005, 2007a; Ding et al., 2014; Ingalls et al., 2017). However, this model was not widely supported by geological evidence, and has not received general consensus. This article fills some of the gaps in our understanding by emphasizing three new aspects so far: (1) the Northern Lhasaplano began to grow north of and behind the Gangdese arc with an intervening low-lying basin, in a similar manner to the Central Andean Plateau that began to grow eastward of magmatic arc with the intervening Altiplano basin (Garzione et al., 2017); (2) the Northern Lhasaplano started to grow >30 m.y. before the onset of the India-Asia collision above an oceanic subduction zone, as is

the case for the modern Central Andean Plateau (Garzione et al., 2017); (3) the Northern Lhasaplano was a wide and relatively thick plateau (Fig. 9), an inference supported by >50% crustal shortening during the Late Cretaceous (Murphy et al., 1997; Kapp et al., 2003, 2007a, 2007b; Volkmer et al., 2007, 2014) and by the large volume of detritus delivered from the central Lhasa terrane to the Xigaze forearc basin since ca. 88 Ma (An et al., 2014).

Despite the lack of paleoelevation estimates for the Northern Lhasaplano, an Andean-style Tibetan plateau model is favored by stable-isotope data from carbonates in the Lhasa terrane, indicating high elevation already in the Paleocene–Eocene (Ding et al., 2014; Xu et al., 2015; Ingalls et al., 2017). The Andes, however, do not have a continental collision zone in its foreland, whereas the Lhasa block was affected not only by oceanic subduction in the south but also by Middle Jurassic to Early Cretaceous collision with Qiangtang in the north (Girardeau et al., 1984; Zhu et al., 2016; Bian et al., 2017; Ma et al., 2017). Compressional tectonic stress consequent to the Lhasa-Qiangtang collision may thus provide an alternative interpretation for the rise of the Northern Lhasaplano and for development and southward propagation of the northern Lhasa thrust belt during the Late Cretaceous. Although future studies are needed to clarify the tectonic mechanism of uplift and to constrain paleoelevation of the Northern Lhasaplano, the Late Cretaceous paleogeography of the southern Tibetan Plateau, including localized deformation and topographic relief in the Northern Lhasaplano, topographic relief in the Gangdese arc, and the intervening basin where the Daxiong Formation was deposited (Fig. 10B), shows remarkable similarity to the early development of the Central Andean Plateau, that includes localized deformation and relief in the Eastern Cordillera, an elevated Andean magmatic arc, and the intervening Altiplano basin at low to moderate paleoelevation (e.g., Garzione et al., 2017 and references therein). The topographic evolution of the Northern Lhasaplano prior to the India-Asia collision may thus be compared with that of other Andean-style plateaus developed above long-lived oceanic subduction zones.

CONCLUSIONS

Alluvial-fan conglomerates and braided-river sandstones of the Jingzhushan and Daxiong formations were deposited in the central and northern Lhasa terranes, where they overlie shallow-marine carbonates deposited until ca. 93 Ma. Rapid terrigenous deposition was ongoing in the early Turonian (ca. 92 Ma). U-Pb ages and in situ Hf isotope signatures of detrital zircons, clastic petrography, and paleocurrent data indicate that the Jingzhushan and Daxiong formations were both derived from the central-northern Lhasa terranes rather than from the BNSZ in the north or Gangdese arc in the south.

Stratigraphic, sedimentological, and provenance analysis, together with broadly coeval activation of the Gaize-Siling Co and Gugu La thrust belts associated with shortening and crustal thickening, indicate that actively eroding highlands fed the Jingzhushan and Daxiong conglomerate-bearing units along its opposite sides at the same time. This elevated source terrane, named the Northern Lhasaplano in this study, experienced prominent and widespread topographic growth beginning at ca. 92 Ma.

The youngest marine strata, provenance change, and tectonic shortening occurred earlier in the northern than in the southern Lhasa terranes, indicating that surface uplift and retreat of seaways progressed southward in time across the BNSZ and Lhasa block. Paleotopography of the Northern Lhasaplano suggests that an Andean-style plateau developed above the Neo-Tethyan subduction zone in Tibet during the Late Cretaceous, preceding the continental collision between India and Asia by more than 30 m.y.

ACKNOWLEDGMENTS

Bin Wu, Zhiyong Zhu, Xiong Yan, Shijie Zhang, and Hanpu Fu are thanked for their help in the analysis of zircon U-Pb ages and Hf isotopes and Bo Zhou, Jiangang Wang, Xiaojian Liu, and Yiwei Xu for their assistance in the field. We are grateful to Joel Saylor and Andrew Laskowski for their helpful comments, to the editors for careful handling, and to reviewers Paul Kapp and Andrew Leier for their helpful advice and constructive suggestions. This study was financially supported by the National Natural Science Foundation of China Projects (91755209, 41472081, 41602104), the Natural Science Foundation of Jiangsu Province (BK20160858), and the U.S. National Science Foundation (1545859). Data for this paper can be accessed from the supporting information.

REFERENCES CITED

An, W., Hu, X., Garzanti, E., BouDagher-Fadel, M.K., Wang, J., and Sun, G., 2014, Xigaze forearc basin revisited (South Tibet): Provenance changes and origin of the Xigaze Ophiolite: Geological Society of America Bulletin, v. 126, no. 11–12, p. 1595–1613, https://doi.org/10.1130/B31020.1.

An, Z., Kutzbach, J.E., Prell, W.L., and Porter, S.C., 2001, Evolution of Asian monsoons and phased uplift of the Himalaya-Tibetan plateau since Late Miocene times: Nature, v. 411, no. 6833, p. 62–66, https://doi.org/10.1038/35075035.

Bian, W., Yang, T., Ma, Y., Jin, J., Gao, F., Zhang, S., Wu, H., and Li, H., 2017, New Early Cretaceous palaeomagnetic and geochronological results from the far western Lhasa terrane: Contributions to the Lhasa-Qiangtang collision: Scientific Reports, v. 7, no. 16216, https://doi.org/10.1038/s41598-017-16482-3.

Blair, T.C., and McPherson, J.G., 1994, Alluvial fans and their natural distinction from rivers based on morphology, hydraulic processes, sedimentary processes, and facies assemblages: Journal of Sedimentary Research, v. 64, no. 3a, p. 450–489, https://doi.org/10.1306/d4267dde-2b26-11d7-8648000102c1865d.

BouDagher-Fadel, M., 2015, Biostratigraphic and Geological Significance of Planktonic Foraminifera: London, UK, UCL Press, 582 p. (updated 2nd edition).

BouDagher-Fadel, M.K., Hu, X.M., Price, G.D., Sun, G.Y., Wang, J.G., and An, W., 2017, Foraminiferal biostratigraphy and palaeoenvironmental analysis of the Mid-Cretaceous limestones in the Southern Tibetan Plateau: Journal of Foraminiferal Research, v. 47, no. 2, p. 188–207.

Chu, M.F., Chung, S.L., Song, B., Liu, D., O'Reilly, S.Y., Pearson, N.J., Ji, J., and Wen, D.J., 2006, Zircon U-Pb and Hf isotope constraints on the Mesozoic tectonics and crustal evolution of southern Tibet: Geology, v. 34, no. 9, p. 745–748, https://doi.org/10.1130/G22725.1.

Chung, S.L., Lo, C.H., Lee, T.Y., Zhang, Y., Xie, Y., Li, X., Wang, K.L., and Wang, P.L., 1998, Diachronous uplift of the Tibetan plateau starting 40 Myr ago: Nature, v. 394, no. 6695, p. 769–773, https://doi.org/10.1038/29511.

DeCelles, P.G., Langford, R.P., and Schwartz, R.K., 1983, Two new methods of palaeocurrent determination from trough cross-stratification: Journal of Sedimentary Petrology, v. 53, p. 629–642.

DeCelles, P.G., Kapp, P., Ding, L., and Gehrels, G., 2007, Late Cretaceous to middle Tertiary basin evolution in the central Tibetan Plateau: Changing environments in response to tectonic partitioning, aridification, and regional elevation gain: Geological Society of America Bulletin, v. 119, no. 5–6, p. 654–680, https://doi.org/10.1130/B26074.1.

Deng, T., Wang, X., Fortelius, M., Li, Q., Wang, Y., Tseng, Z.J., Takeuchi, G.T., Saylor, J.E., Säilä, L.K., and Xie, G., 2011, Out of Tibet: Pliocene woolly rhino suggests high-plateau origin of Ice Age megaherbivores: Science, v. 333, no. 6047, p. 1285–1288, https://doi.org/10.1126/science.1206594.

Dickinson, W.R., and Gehrels, G.E., 2009, Use of U-Pb ages of detrital zircons to infer maximum depositional ages of strata: A test against a Colorado Plateau Mesozoic database: Earth and Planetary Science Letters, v. 288, no. 1, p. 115–125, https://doi.org/10.1016/j.epsl.2009.09.013.

Ding, L., Xu, Q., Yue, Y., Wang, H., Cai, F., and Li, S., 2014, The Andean-type Gangdese Mountains: Paleoelevation record from the Paleocene–Eocene Linzhou Basin: Earth and Planetary Science Letters, v. 392, p. 250–264, https://doi.org/10.1016/j.epsl.2014.01.045.

Dupont-Nivet, G., Krijgsman, W., Langereis, C.G., Abels, H.A., Dai, S., and Fang, X., 2007, Tibetan plateau aridification linked to global cooling at the Eocene–Oligocene transition: Nature, v. 445, no. 7128, p. 635–638, https://doi.org/10.1038/nature05516.

England, P., and Searle, M., 1986, The Cretaceous-Tertiary deformation of the Lhasa block and its implications for crustal thickening in Tibet: Tectonics, v. 5, p. 1–14, https://doi.org/10.1029/TC005i001p00001.

Garzanti, E., 2016, From static to dynamic provenance analysis: Sedimentary petrology upgraded: Sedimentary Geology, v. 336, p. 3–13, https://doi.org/10.1016/j.sedgeo.2015.07.010.

Garzione, C.N., McQuarrie, N., Perez, N.D., Ehlers, T.A., Beck, S.L., Kar, N., Eichelberger, N., Chapman, A.D., Ward, K.M., and Ducea, M.N., 2017, Tectonic evolution of the Central Andean Plateau and implications for the growth of plateaus: Annual Review of Earth and Planetary Sciences, v. 45, p. 529–559, https://doi.org/10.1146/annurev-earth-063016-020612.

Gehrels, G., Kapp, P., DeCelles, P., Pullen, A., Blakey, R., Weislogel, A., Ding, L., Guynn, J., Martin, A., and McQuarrie, N., 2011, Detrital zircon geochronology of pre-Tertiary strata in the Tibetan-Himalayan orogen: Tectonics, v. 30, no. 5, https://doi.org/10.1029/2011TC002868.

Girardeau, J., Marcoux, J., Allegre, C.J., Bassoullet, J.P., Youking, T., Xuchang, X., Yougong, Z., and Xibin, W., 1984, Tectonic environment and geodynamic significance of the Neo-Cimmerian Donqiao ophiolite, Bangong-Nujiang suture zone, Tibet: Nature, v. 307, no. 5946, p. 27–31, https://doi.org/10.1038/307027a0.

Haq, B.U., 2014, Cretaceous eustasy revisited: Global and Planetary Change, v. 113, no. 2, p. 44–58, https://doi.org/10.1016/j.gloplacha.2013.12.007.

Hetzel, R., Dunkl, I., Haider, V., Strobl, M., von Eynatten, H., Ding, L., and Frei, D., 2011, Peneplain formation in southern Tibet predates the India-Asia collision and plateau uplift: Geology, v. 39, p. 983–986, https://doi.org/10.1130/G32069.1.

Hu, X., Garzanti, E., Moore, T., and Raffi, I., 2015, Direct stratigraphic dating of India-Asia collision onset at the Selandian (middle Paleocene, 59 ± 1 Ma): Geology, v. 43, no. 10, p. 859–862, https://doi.org/10.1130/G36872.1.

Ingalls, M., Rowley, D., Olack, G., Currie, B., Li, S., Schmidt, J., Tremblay, M., Polissar, P., Shuster, D.L., Lin, D., and Colman, A., 2017, Paleocene to Pliocene low-latitude, high-elevation basins of southern Tibet: Implications for tectonic models of India-Asia collision, Cenozoic climate, and geochemical weathering: Geological Society of America Bulletin, v. 130, no. 1–2, p. 307–330, https://doi.org/10.1130/B31723.1.

Jackson, S.E., Pearson, N.J., Griffin, W.L., and Belousova, E.A., 2004, The application of laser ablation-inductively coupled plasma-mass spectrometry to in situ U-Pb zircon geochronology: Chemical Geology, v. 211, no. 1, p. 47–69, https://doi.org/10.1016/j.chemgeo.2004.06.017.

Ji, W.Q., Wu, F.Y., Chung, S.L., Li, J.X., and Liu, C.Z., 2009, Zircon U–Pb geochronology and Hf isotopic constraints on petrogenesis of the Gangdese batholith, southern Tibet: Chemical Geology, v. 262, no. 3–4, p. 229–245, https://doi.org/10.1016/j.chemgeo.2009.01.020.

Kapp, P., Murphy, M.A., Yin, A., Harrison, T.M., Ding, L., and Guo, J., 2003, Mesozoic and Cenozoic tectonic evolution of the Shiquanhe area of western Tibet: Tectonics, v. 22, no. 4, https://doi.org/10.1029/2001TC001332.

Kapp, P., Yin, A., Harrison, T.M., and Ding, L., 2005, Cretaceous-Tertiary shortening, basin development, and volcanism in central Tibet: Geological Society of America Bulletin, v. 117, no. 7–8, p. 865–878, https://doi.org/10.1130/B25595.1.

Kapp, P., DeCelles, P., Leier, A., Fabijanic, J., He, S., Pullen, A., Gehrels, G., and Ding, L., 2007a, The Gangdese retroarc thrust belt revealed: GSA Today, v. 17, no. 7, p. 4–9, https://doi.org/10.1130/GSAT01707A.1.

Kapp, P., DeCelles, P.G., Gehrels, G.E., Heizler, M., and Ding, L., 2007b, Geological records of the Lhasa-Qiangtang and Indo-Asian collisions in the Nima area of central Tibet: Geological Society of America Bulletin, v. 119, no. 7–8, p. 917–933, https://doi.org/10.1130/B26033.1.

Leier, A.L., DeCelles, P.G., Kapp, P., and Gehrels, G.E., 2007a, Lower Cretaceous strata in the Lhasa terrane, Tibet, with implications for understanding the early tectonic history of the Tibetan Plateau: Journal of Sedimentary Research, v. 77, no. 10, p. 809–825, https://doi.org/10.2110/jsr.2007.078.

Leier, A.L., Kapp, P., Gehrels, G.E., and DeCelles, P.G., 2007b, Detrital zircon geochronology of Carboniferous–Cretaceous strata in the Lhasa terrane, Southern Tibet: Basin Research, v. 19, no. 3, p. 361–378, https://doi.org/10.1111/j.1365-2117.2007.00330.x.

Li, H., Yang, S., Li, D., Zhang, S., Lv, Z., and Chen, G., 2014a, Geochronology, geochemistry, tectonic setting and metallogenetic significance of the Late Cretaceous quartz monzonite in the northwestern Gangdise terrane (in Chinese with English abstract): Geotectonica Et Metallogenia, v. 38, no. 3, p. 694–705.

Li, J.X., Qin, K.Z., Li, G.M., Richards, J.P., Zhao, J.X., and Cao, M.J., 2014b, Geochronology, geochemistry, and zircon Hf isotopic compositions of Mesozoic intermediate-felsic intrusions in central Tibet: Petrogenetic and tectonic implications: Lithos, v. 198–199, p. 77–91, https://doi.org/10.1016/j.lithos.2014.03.025.

Liu, D., Shi, R., Ding, L., Huang, Q., Zhang, X., Yue, Y., and Zhang, L., 2017, Zircon U-Pb age and Hf isotopic compositions of Mesozoic granitoids in southern Qiangtang, Tibet: Implications for the subduction of the Bangong-Nujiang Tethyan Ocean: Gondwana Research, v. 41, p. 157–172, https://doi.org/10.1016/j.gr.2015.04.007.

Ma, A., Hu, X., Garzanti, E., Han, Z., and Lai, W., 2017, Sedimentary and tectonic evolution of the southern Qiangtang basin: Implications for the Lhasa-Qiangtang collision timing: Mesozoic geology of central Tibet: Journal of Geophysical Research. Solid Earth, v. 122, p. 4790–4813, https://doi.org/10.1002/2017JB014211.

Ma, A., Hu, X., Kapp, P., Han, Z., Lai, W., and BouDagher-Fadel, M., 2018, The disappearance of a Late Jurassic remnant sea in the southern Qiangtang Block (Shamuluo Formation, Najiangco area): Implications for the tectonic uplift of central Tibet: Palaeogeography, Palaeoclimatology, Palaeoecology, v. 506, p. 30–47, https://doi.org/10.1016/j.palaeo.2018.06.005.

Miall, A.D., 1996, The Geology of Fluvial Deposits: Sedimentary Facies, Basin Analysis, and Petroleum Geology: New York, USA, Springer Publishing, 582 p.

Molnar, P., England, P., and Martinod, J., 1993, Mantle dynamics, uplift of the Tibetan Plateau, and the Indian monsoon: Reviews of Geophysics, v. 31, no. 4, p. 357–396, https://doi.org/10.1029/93RG02030.

Murphy, M.A., Yin, A., Harrison, T.M., Dürr, S.B., Chen, Z., Ryerson, F.J., Kidd, W.S.F., Wang, X., and Zhou, X., 1997, Did the Indo-Asian collision alone create the Tibetan plateau?: Geology, v. 25, p. 719–722, https://doi.org/10.1130/0091-7613(1997)025<0719:DTIACA>2.3.CO;2.

Orme, D.A., and Laskowski, A.K., 2016, Basin Analysis of the Albian–Santonian Xigaze Forearc, Lazi Region, South-Central Tibet: Journal of Sedimentary Research, v. 86, no. 8, p. 894–913, https://doi.org/10.2110/jsr.2016.59.

Pan, G. T., Ding, J., Yao, D. S., and Wang, L. Q., 2004, Geological map of the Qinghai-Xizang (Tibet) Plateau and adjacent areas: China, Chengdu Cartographic Publishing House.

Pullen, A., Kapp, P., Gehrels, G.E., Vervoort, J.D., and Ding, L., 2008, Triassic continental subduction in central Tibet and Mediterranean-style closure of the Paleo-Tethys Ocean: Geology, v. 36, no. 5, p. 351–354, https://doi.org/10.1130/G24435A.1.

Pullen, A., Kapp, P., Gehrels, G.E., Ding, L., and Zhang, Q., 2011, Metamorphic rocks in central Tibet: Lateral variations and implications for crustal structure: Geological Society of America Bulletin, v. 123, no. 3–4, p. 585–600, https://doi.org/10.1130/B30154.1.

Raymo, M.E., and Ruddiman, W.F., 1992, Tectonic forcing of Late Cenozoic climate: Nature, v. 359, p. 117–122, https://doi.org/10.1038/359117a0.

Rohrmann, A., Kapp, P., Carrapa, B., Reiners, P.W., Guynn, J., Ding, L., and Heizler, M., 2012, Thermochronologic evidence for plateau formation in central Tibet by 45 Ma: Geology, v. 40, p. 187–190, https://doi.org/10.1130/G32530.1.

Rose, W.I., and Durant, A.J., 2011, Fate of volcanic ash: Aggregation and fallout: Geology, v. 39, no. 9, p. 895–896, https://doi.org/10.1130/focus092011.1.

Rowley, D., and Currie, B., 2006, Paleo-altimetry of the Late Eocene to Miocene Lunpola basin, central Tibet: Nature, v. 439, p. 677–681, https://doi.org/10.1038/nature04506.

Sarna-Wojcicki, A.M., Shipley, S., Waitt, R.B., Jr., Dzurisin, D., and Wood, S.H., 1981, Areal distribution, thickness, mass, volume, and grain size of air-fall ash from the six major eruptions of 1980, *in* Lipman, P.W., and Mullineaux, D.R., eds., The 1980 Eruptions of Mount St. Helens, Washington: U.S. Geological Survey Professional Paper, v. 1250, p. 577–599.

Sun, G., Hu, X., Sinclair, H.D., BouDagher-Fadel, M.K., and Wang, J., 2015a, Late Cretaceous evolution of the Coqen Basin (Lhasa terrane) and implications for early topographic growth on the Tibetan Plateau: Geological Society of America Bulletin, v. 127, no. 7–8, p. 1001–1020, https://doi.org/10.1130/b31137.1.

Sun, G.Y., Hu, X.M., Zhu, D.C., Hong, W.T., Wang, J.G., and Wang, Q., 2015b, Thickened juvenile lower crust-derived ~ 90 Ma adakitic rocks in the central Lhasa terrane, Tibet: Lithos, v. 224–225, p. 225–239, https://doi.org/10.1016/j.lithos.2015.03.010.

Sun, G., Hu, X., and Sinclair, H.D., 2017, Early Cretaceous palaeogeographic evolution of the Coqen Basin in the Lhasa Terrane, southern Tibetan Plateau: Palaeogeography, Palaeoclimatology, Palaeoecology, v. 485, p. 101–118, https://doi.org/10.1016/j.palaeo.2017.06.006.

Volkmer, J.E., Kapp, P., Guynn, J.H., and Lai, Q., 2007, Cretaceous-Tertiary structural evolution of the north central Lhasa terrane, Tibet: Tectonics, v. 26, no. 6, https://doi.org/10.1029/2005TC001832.

Volkmer, J.E., Kapp, P., Horton, B.K., Gehrels, G.E., Minervini, J.M., and Ding, L., 2014, Northern Lhasa thrust belt of central Tibet: Evidence of Cretaceous–early Cenozoic shortening within a passive roof thrust system?, *in* Nie, J., Horton, B.K., and Hoke, G.D., eds., Toward an Improved Understanding of Uplift Mechanisms and the Elevation History of the Tibetan Plateau: Geological Society of America Special Paper 507, p. 59–70, https://doi.org/10.1130/2014.2507(03).

Wang, C., Zhao, X., Liu, Z., Lippert, P.C., Graham, S.A., Coe, R.S., Yi, H., Zhu, L., Liu, S., and Li, Y., 2008, Constraints on the early uplift history of the Tibetan Plateau: Proceedings of the National Academy of Sciences of the United States of America, v. 105, p. 4987–4992, https://doi.org/10.1073/pnas.0703595105.

Wang, C., Dai, J., Zhao, X., Li, Y., Graham, S., He, D., Ran, B., and Meng, J., 2014, Outward-growth of the Tibetan Plateau during the Cenozoic: A review: Tectonophysics, v. 621, p. 1–43, https://doi.org/10.1016/j.tecto.2014.01.036.

Wang, J.G., Hu, X., Garzanti, E., Ji, W.Q., Liu, Z.C., Liu, X.C., and Wu, F.Y., 2017, Early Cretaceous topographic growth of the Lhasaplano, Tibetan Plateau: Constraints from the Damxung Conglomerate: Journal of Geophysical Research. Solid Earth, v. 122, no. 7, p. 5748–5765, https://doi.org/10.1002/2017JB014278.

Xu, Q., Ding, L., Hetzel, R., Yue, Y., and Rades, E.F., 2015, Low elevation of the northern Lhasa terrane in the Eocene: Implications for relief development in south Tibet: Terra Nova, v. 27, no. 6, p. 458–466, https://doi.org/10.1111/ter.12180.

XZBGM, 1993, Regional Geology of Tibet Autonomous Region (in Chinese), Beijing, China, Geological Publishing House.

Zhang, Q., Ding, L., Cai, F., Xu, X., Zhang, L., Xu, Q., and Willems, H., 2011, Early Cretaceous Gangdese retroarc foreland basin evolution in the Selin Co basin, central Tibet: Evidence from sedimentology and detrital zircon geochronology, *in* Gloaguen, R., and Ratschbacher, L., eds., Growth and Collapse of the Tibetan Plateau: Geological Society of London, Special Publication 353, no. 1, p. 27–44, https://doi.org/10.1144/SP353.3.

Zhu, D.C., Li, S.M., Cawood, P.A., Wang, Q., Zhao, Z.D., Liu, S.A., and Wang, L.Q., 2016, Assembly of the Lhasa and Qiangtang terranes in central Tibet by divergent double subduction: Lithos, v. 245, p. 7–17, https://doi.org/10.1016/j.lithos.2015.06.023.

Zhu, D.C., Zhao, Z.D., Niu, Y., Dilek, Y., and Mo, X.X., 2011a, Lhasa terrane in southern Tibet came from Australia: Geology, v. 39, no. 8, p. 727–730, https://doi.org/10.1130/G31895.1.

Zhu, D.C., Zhao, Z.D., Niu, Y., Mo, X.X., Chung, S.L., Hou, Z.Q., Wang, L.Q., and Wu, F.-Y., 2011b, The Lhasa Terrane: Record of a microcontinent and its histories of drift and growth: Earth and Planetary Science Letters, v. 301, no. 1, p. 241–255, https://doi.org/10.1016/j.epsl.2010.11.005.

Zhu, D.C., Wang, Q., Cawood, P.A., Zhao, Z.D., and Mo, X.X., 2017, Raising the Gangdese Mountains in southern Tibet: Journal of Geophysical Research. Solid Earth, v. 122, p. 214–223, https://doi.org/10.1002/2016JB013508.

Zhu, D.C., Wang, Q., Zhao, Z.D., Chung, S.L., Cawood, P.A., Niu, Y., Liu, S.A., Wu, F.Y., and Mo, X.X., 2015, Magmatic record of India-Asia collision: Scientific Reports, v. 5, no. 14289, https://doi.org/10.1038/srep14289 (Corrigendum: http://dx.doi.org/10.1038/srep17236).

Science Editor: Rob Strachan
Associate Editor: Brian McConnell

Manuscript Received 28 August 2018
Revised Manuscript Received 11 December 2018
Manuscript Accepted 1 February 2019

Printed in the USA